What drives microplate motion and deformation in the northeastern Caribbean plate boundary region ?

Steven van Benthem, Rob Govers and Rinus Wortel

r.govers@uu.nl, Department of Earth Sciences, Utrecht University, The Netherlands

submitted to *Tectonics* June 28 2013

revised version submitted to *Tectonics* March 2014

This article has been accepted for publication and undergone full peer review but has not been through the copyediting, typesetting, pagination and proofreading process which may lead to differences between this version and the Version of Record. Please cite this article as doi: 10.1002/2013TC003402

1. Abstract

The north Caribbean plate boundary zone is a broad deformation zone with several fault systems and tectonic blocks that move with different velocities. The indentation by the Bahamas Platform (the "Bahamas Collision") is generally invoked as a cause of this fragmentation. We propose that a second driver of deformation is the western edge of the south-dipping Puerto Rico slab moving sideways with the North America plate. The westward motion of the slab edge results in a push on the Caribbean plate further west. We refer to this second mechanism for deformation as "Slab Edge Push". The motion of the North America plate relative to the Caribbean plate causes both drivers to migrate from east to west. The Bahamas Collision and Slab Edge Push have been operating simultaneously since the Miocene. The question is the relative importance of the two mechanisms. We use mechanical finite element models that represent the two mechanisms from the Late Oligocene (30 Ma) to the Present. For the Present, both models successfully reproduce observed deformation, implying that both models are viable. Back in time the Slab Edge Push mechanism better reproduces observations. Neither mechanism successfully reproduces the observed Miocene counter-clockwise rotation of Puerto Rico. We use this rotation to tune a final model that includes fractional contributions of both mechanisms. We find that the Slab Edge Push was the dominant driver of deformation in the north Caribbean plate boundary zone since 30 Ma.

2. Introduction

The small Caribbean plate (inset Figure 1) is mainly oceanic. It is bounded by subduction systems at its eastern and western plate boundaries, and by transpressional shear systems at its northern and southern boundaries [*Molnar and Sykes*, 1969]. The tectonics of the northern plate boundary zone (Figure 1), which separates the Caribbean plate from the North America plate, are diverse and complicated. The westward subduction of the North America plate at the northern Lesser Antilles changes to highly oblique subduction at the Puerto Rico Trench [*Molnar and Sykes*, 1969; *Vening Meinesz et al.*, 1934] and to strain partitioning north of Hispaniola [*Calais et al.*, 2002], with strike-slip motion being accommodated at the Septentrional Fault and trench-perpendicular motion accommodated along the North Hispaniola Deformed Belt [NHDB, *Dillon et al.*, 1992]. West of Hispaniola, relative plate motion is strike-slip at the Oriente and Swan transform fault zones [*Dillon et al.*, 1992].

The relative motion between the stable, more interior part of the Caribbean plate and the plate boundary zone to the north of it is mainly accommodated along the Muertos Trough and the Enriquillo-Plantain Garden fault zone. This “northeastern Caribbean plate boundary zone” has a north-south extent of ~200 km and consists of smaller blocks or “microplates”. From west to east these are the Gonave microplate [*Rosencrantz and Mann*, 1991], the Hispaniola microplate [*Mann et al.*, 2002] and the Puerto Rico - Virgin Islands microplate [*Byrne et al.*, 1985]. The Hispaniola and Gonave microplates currently move with a velocity that is intermediate between velocities of the North America and Caribbean plates [*DeMets and Wiggins-Grandison*, 2007; *Manaker et al.*, 2008], while the Puerto Rico - Virgin Islands microplate is hardly moving with respect to the Caribbean plate [*Jansma et al.*, 2000]. Question is why the northeastern Caribbean plate boundary zone is so wide and fragmented. As we will argue below, the answer involves the fact that the structure of the plate boundary changes diachronously which introduces spatial-temporal variations in the forces acting at the plate boundary.

The Bahamas Platform on the North America plate stands out amongst the surrounding sea floor as a result of a relatively thick crust that is covered by carbonates. The collision or (oblique)

subduction of the Bahamas Platform beneath the Caribbean plate, hereafter refered to as "Bahamas Collision", is usually invoked to explain differential velocities in the northeastern Caribbean plate boundary zone [*Mann et al.*, 2002]. The Bahamas Platform itself, however, shows no signs of significant deformation besides some normal faulting [*Dolan et al.*, 1998]. Rocks derived from the Bahamas Platform have not been found on Hispaniola, as was the case for the Eocene collision of Cuba with the Bahamas Platform [*Pardo*, 1975]. This suggests that the present collision is "soft", i.e., that the collision forces on the Caribbean plate and vice versa are relatively small and that the Bahamas Platform alone is unlikely to explain the observed fragmentation of the northeastern Caribbean plate boundary zone. Another concern of identifying the collision the Bahamas Platform as the sole driver of northeastern Caribbean tectonics has to do with timing. The collision is thought to have started somewhere between the Middle Miocene and Pliocene [*de Zoeten and Mann*, 1991; *Dolan et al.*, 1998; *Grindlay et al.*, 2005]. Prior to the collision, mechanical interaction between the North America and Caribbean plates consisted of frictional relative motion. Significant deformation has occurred in the northeastern Caribbean plate boundary zone since the start of the Cenozoic, e.g., 24º of Miocene counter-clockwise (CCW) rotation of Puerto Rico [*Reid et al.*, 1991], large Cenozoic CCW rotation of Hispaniola [*Vincenz and Dasgupta*, 1978], Oligocene-Present rifting in the Mona Rift [*Mondziel et al.*, 2010] and ~100 km of Miocene – Present convergence at the Muertos Trough [*Masson and Scanlon*, 1991] as is suggested by seismicity [*Byrne et al.*, 1985] and seismic tomography [*van Benthem et al.*, 2013]. It is therefore questionable that the collision of the Bahamas Platform alone can explain the tectonic evolution of the northeastern Caribbean plate boundary region since the Eocene/Oligocene.

Molnar and Sykes [1969] propose the existence of a laterally moving slab along the northern plate boundary, brought in by westward subduction at the Lesser Antilles. Seismic tomography results support the presence of such a slab, with a distinct western edge [*van Benthem et al.*, 2013]. We propose that the westward motion of the lateral edge of this slab is an additional driver of microplate motion since the Eocene. We refer to this driving mechanism as the "Slab Edge Push".

In this paper we construct mechanical (finite element) models based on these two drivers. Importantly, the total force exerted by either mechanism (or combinations of them) is constrained by the results of our previous modeling study [*van Benthem and Govers*, 2010]. Here, we first investigate

separately the impact of Bahamas Collision and Slab Edge Push on the secular deformation and microplate motion of the northeastern Caribbean plate boundary zone. We will see that neither mechanism can individually explain available observations. Next, we use geological observations to constrain their combined contributions.

Most of the published mechanical models of the region are kinematically driven, with a focus on the seismic cycle time scale [*Ali et al.*, 2008; *Manaker et al.*, 2008; *ten Brink and López-Venegas*, 2012]. Force driven models are more suitable for answering our research question. In this category, studies by Van Benthem and Govers [2010] and Negredo et al. [2004] focus on the forces that dominate the dynamics of the Caribbean plate at present. There have been no studies thus far that quantify the evolution of the Bahamas Collision force or its associated deformation. Thus, quantitative modeling of the driving mechanism is a novel element for both the Slab Edge Push scenario proposed here, and for the existing Bahamas Collision scenario. In the next section we present the most pertinent evidence that is relevant for setting up the mechanical models in the context of the tectonic evolution of the region.

3. Mechanisms for plate boundary deformation in the north-eastern Caribbean

Bahamas Collision

Evidence for the Bahamas Collision is based on (1) observed Pliocene-Present deformation in Hispaniola [*de Zoeten and Mann*, 1991], (2) the occurrence of unusually large thrust earthquakes along the plate contact between Hispaniola and the Bahamas Platform compared to seismicity further away along the plate boundary [*Dolan and Wald*, 1998] and (3) anomalous bathymetry along the plate boundary [*Dolan et al.*, 1998]. Also elastic block modeling of GPS velocities [*Manaker et al.*, 2008] indicate that a higher frictional coupling is needed to the north of Hispaniola to reproduce GPS-derived velocities here.

The northeastern Caribbean plate boundary came into existence following an Eocene plate boundary reorganization of the Great Arc of the Caribbean. The northern slab segment of the Great Arc of the Caribbean broke away from the rest of what then became the Lesser Antilles slab. The tearing process created an (approximately) vertical edge of the slab that since then has migrated beneath Hispaniola. The relative motion of the Caribbean and North America plates along the new east-west plate boundary was left-lateral with a small component of convergence. This convergence resulted in slow, continued subduction to the east of the slab edge. West of the slab edge, some of the ~200 km post-Eocene convergence may have been accommodated along the former subduction plate contact. De Zoeten and Mann [1991] propose that this slow subduction eventually led to collision of the Bahamas Platform with Hispaniola in the Pliocene. The contact area was probably small at first, and increased with time as oblique convergence continued, eventually resulting in thrusting and uplift. The westward motion of the Bahamas Platform with the North America plate implies that collision migrates from east to west with respect to the Caribbean plate.

Bahamas Collision is commonly held responsible for the segmentation into microplates of the north Caribbean plate boundary zone, for instance that Hispaniola started to move together with North America to the west, while the Puerto Rico / Virgin Islands microplate stayed behind, moving with the Caribbean plate. Figure 2 shows Bahamas Collision in the present-day configuration. Here it results in a traction on the near-vertical strike-slip interface between the North America and Caribbean plates (blue) that acts in the direction of relative motion.

Slab Edge Push

The edge of the Puerto Rico – Lesser Antilles slab is presently located beneath east Hispaniola between 69º and 70ºW [*Dolan et al.*, 1998; *van Benthem et al.*, 2013]. Figure 2 shows the geometry of the present-day slab beneath the northeastern Caribbean region. The figure does not show the vertical tear in the slab between 50 and 150 km depth that was recently discovered by Meighan et al. [2013]. The plate boundary east of Hispaniola is a south dipping subduction fault [*Dolan and Wald*, 1998], accommodating highly oblique convergence. West of Hispaniola the plate boundary is a vertical fault [*Calais et al.*, 1998], which accommodates left-lateral transpression. The westward transport of the shallow part of the slab with the North America plate is hindered by the existence of Caribbean lithosphere further to the west. Deformation of Caribbean lithosphere is needed to allow continued westward transport of the slab. The red area in Figure 2 denotes the area where the slab edge exerts a traction on the Caribbean plate in the direction of relative plate motion.

A similar, yet not identical, tectonic setting was identified by Furlong and Govers [1999] at the southern edge of the Juan de Fuca slab near the Mendocino triple junction. Sideways motion of the slab results in significant deformation of the overriding North America plate. The Juan de Fuca slab moves away from the North America mantle adjacent to the slab, thus opening a slab gap. This is a critical difference with respect to the tectonic setting of Hispaniola, where the slab edge converges with Caribbean lithosphere.

The Eocene plate boundary reorganization that ended with the slab edge beneath Hispaniola resulted from breakoff of the Cuban slab segment of the Great Arc of the Caribbean. The slab edge mi-

grated westward, together with the North America lithosphere at the surface. This implies that Slab Edge Push first acted on the eastern part of the northeastern Caribbean plate boundary zone and later on more western parts of it.

Two mechanisms acting in concert

In view of the reconstruction of the areal distribution of the Bahamas Platform [*Dolan et al*., 1998], the imaging results for the slab edge [*van Benthem et al*., 2013] and the regional plate kinematics, we must consider the distinct possibilty that Bahamas Collision and Slab Edge Push have been, and continue to be, operating simultaneously. At present the North-America-Caribbean plate boundary dips gently towards the south near Puerto Rico. South of Cuba, relative motion is strike-slip, and the plate boundary is vertical [*Calais et al.*, 1998]. The orientation and nature of the plate boundary thus changes in the Hispaniola plate boundary segment. Together with the North America plate this transition has been migrating to the west relative to the Caribbean plate. Slab Edge Push drives deformation associated with this plate boundary reorganization. As a consequence, even if the Bahamas Collision turns out to be the main driver of deformation of the northeastern Caribbean plate boundary zone, some contribution of Slab Edge Push appears to be required.

For both drivers we benefit from constraints on the direction and magnitude of the force that were derived in a previous modeling study [*van Benthem and Govers, 2010*]. From torque balance of the entire Caribbean plate, these authors found upper and lower limits on the force exerted by the North America plate along the north Caribbean plate boundary. The fact that they found a range rather than a single value resulted from uncertainties in especially the trench suction force by the Lesser Antilles slab on the Caribbean plate. Here, the total force by Bahamas Collision and Slab Edge Push is required to fall within this range.

The question is the relative importance of the two driving mechanisms. In section 4, we therefore formulate mechanical models that are based on either the Bahamas Collision or the Slab Edge Push scenario. After analyzing these models separately in sections 5 and 6, we will return to the question of the relative significance of the two drivers in section 7.

4. Model setup

To evaluate the deformation of the northeastern Caribbean plate boundary zone due to both scenarios, we construct mechanical models. As will be explained below, we choose simple model setups, so that most of the ingredients can be a priori constrained by observations. Despite this, some model parameters (notably fault friction and average viscosity of the region) need additional constraints. Therefore, we use model results for the Present-day in combination with observations to tune these parameters for the northeastern Caribbean plate boundary zone (Section 5). These parameters are then used in models for the period 30-2.5 Ma (Section 6), which covers a significant part of the evolution of the plate boundary zone, however, excluding the plate boundary reorganization period 42-30 Ma.

Our mechanical model straddles the northeast Caribbean plate boundary region (red rectangle in Figure 3a). Given the large horizontal extent of the model region the lithosphere is represented by a spherical shell with an earth radius and uniform thickness of 100 km. As we will see below, regional observations of deformation have only limited depth information and for this reason we restrict the model to be 2D plane stress. We use finite element package GTECTON to solve the mechanical equilibrium equations [Govers and Meijer, 2001]. The boundary conditions section (below) details how we incorporate depth variations in our 2D models. We use linear rheologies in the mechanical models. The resulting displacements strain (rates), velocities, stresses, vertical axis rotation (rates), uplift (rates), and slip on regional faults represent averages over lithospheric thickness.

Domain and material properties

We use a rectangular spherical shell to represent the region (55-84 ºW, 13-26 ºN) straddling the northeastern Caribbean plate boundary zone (Figure 3b). The locations and geometry of the plate boundary and major faults are derived from the geological map of French and Schenk [2004]. The spherical model shell has a uniform reference thickness of 100 km and a linear visco-elastic rheology with a Young's modulus of 70 GPa and a Poisson's ratio of 0.25 [*Turcotte and Schubert*, 2002]. We

assume a uniform viscosity. Using a variable viscosity might introduce ambiguity in the interpretation of the results, because it would be difficult to discriminate whether model results stems from the viscosity- or from the force-distribution. The average regional viscosity is not known and is determined by a best fit to Present-day observations (Section 5).

Boundary conditions for the Present-day models

Deformation in the northeastern Caribbean plate boundary zone results from forces acting on the plate boundary zone. Van Benthem and Govers [2010] determined consistent plate boundary forces on the Caribbean-North America plate boundary on the basis of mechanical balance of the Caribbean plate (we refer to these as "line forces"). However, some of the line forces were interdependent and could not be solved for independently: 1) the line force on the north Caribbean plate boundary shows a tradeoff with trench suction along the southern Lesser Antilles, and 2) they could not distinguish between plate boundary friction along the Puerto Rico plate contact and collision at the Bahamas Platform. Van Benthem and Govers [2010] therefore presented all line force sets that were physically possible and that agreed with available (stress) observations (Table 1). Here, we evaluate all their line force sets. The nomenclature of the line force sets is as follows: LOTSUC stands for "a lot of trench suction" at the southern Lesser Antilles Trench, corresponding with a line force of 0.9 TN/m, (2) TSUC stands for "trench suction" at the southern Lesser Antilles Trench, corresponding with a line force of 0.45 TN/m, (3) NOTSUC stands for "no trench suction" at the southern Lesser Antilles Trench. The number in the name stands for *R*, which represents the ratio of σ_{bah} and the magnitude of the frictional traction along the non-collisional section of the Puerto Rico Trench. The magnitudes for the line force sets are listed in Table 2. The directions of the forces are in the direction of relative motion with respect to the Caribbean plate. We will use line force set TSUC5 to illustrate our approach in the following sections.

The line forces need to be converted to tractions that will be imposed on our plane stress deformation models. Consider a subduction interface with a shear traction (Pascal) that varies along the plate contact. When integrated along the downdip length of the subduction interface, this traction

amounts to a line force (Newton/meter) that is oriented opposite to the relative motion direction. The line force will consequently have a dipping orientation. With our 2D model approach we essentially work with depth averages of stress and strain. Consistent with this, the translation of the line forces (Table 2) to traction boundary conditions on the plane stress model is based on the assumption that the tractions are uniform with depth. The dip of subduction interfaces is relatively small, so that we may assume tractions to act in a horizontal direction. These tractions act uniformly on the horizontal projection of the contact area between the subducting and the overriding plate. Converting line forces to average tractions is simpler for vertical interfaces, e.g., transform plate boundaries: dividing the line force by the thickness of the deformation model (100 km). This average traction is imposed directly on the boundary where it acts in the deformation model.

Van Benthem and Govers [2010] solved for the collision line force on the northeast Caribbean plate boundary region. They attribute this line force to the traction due to collision of the Bahamas Platform. We now consider Slab Edge Push to be a good alternative explanation for this line force. This does require some extra explanation, however, because of the nature of their original result. Like the Bahamas Collision, the line force for the Slab Edge Push acts in the North America-Caribbean relative motion direction. Our alternative interpretation of Slab Edge Push results in a slightly different location where the line force acts (see Figures 1 and 3).

Because the analysis of van Benthem and Govers [2010] was based on balance of torques about the center of the earth it is important to evaluate the change in torque for the Slab Edge Push, otherwise the Caribbean Plate may no longer be in mechanical equilibrium. The present-day position of the vertical slab edge lies between 69º-70ºW [*Dolan et al*., 1998; *van Benthem et al.,* 2013]. In the present-day model we assume the slab edge to be located at 69 ºW (Figure 3a). Recognizing that the torque is the product of line force and the length along the surface of the contact over which it acts, we increase the line force for the slab edge push because it acts on a smaller contact. We compute the torque corresponding to the slab edge push, and find that it hardly differs from the original torque that van Benthem and Govers [2010] found for the Bahamas Collision. The Caribbean plate is thus mechanically balanced for the slab edge push force as it is for the Bahamas Collision.

We neglect gravitational topography forces, which are relatively small in magnitude in this

region. We work in the Caribbean reference frame, implying that the southern boundary of the Caribbean lithosphere in our domain is fixed. Far-field forces (ridge push, mantle drag, frictional forces) that drive the North America plate to the west are represented by velocity boundary conditions along the northern edge of our domain [*Richardson and Reding*, 1991].

Boundary conditions for models for 30-2.5 Ma

We use published opening rates of the Cayman Trough [*Leroy et al.*, 2000] to reconstruct the North America plate, including the Bahamas Platform and the slab edge, to its paleo-positions relative to the Caribbean plate. The westward movement of the slab that subducted at the Lesser Antilles results in a westward diachronous change of the (vertical) transform boundary to a dipping subduction contact along the northern plate boundary. We assume that Hispaniola and Puerto Rico-Virgin Islands are independent blocks, surrounded by the same active faults as today [*Dolan et al.*, 1998]. We also assume that forces acting on the Caribbean and other parameters (e.g., viscosity, kinematic fault friction) are equal to the present. This is supported by the stable relative and absolute velocities since the Eocene [*Müller et al.*, 1999]. Like for the Present-day models, we use line force set TSUC5 to illustrate our approach in the following sections. The model setups at 30, 20, 15 and 5 Ma are shown in Figure 3b, as well in the supplementary movie "bcs.mov".

Regional faults/shear zones in the Caribbean plate

Faults are incorporated in the finite element models using a slippery node technique [*Melosh and Williams*, 1989]. This allows fault slip when shear tractions exceed the imposed fault friction. The faults in the model are idealized (infinitely thin, smoothed and continuous) representations of irregular, finite width, anastomosing fault fragments that constitute real fault zones. The irregularities, at both micro and macro scales, cause frictional shear stresses that are relaxed by the periodic release of seismic energy. This ensures that stresses do not build up infinitely, and results in mechanical coupling of plate velocities across faults on geological time scales. This behavior can be simulated with a

(one dimensional) Maxwell model, in which a spring and dashpot are connected in series [*Plattner et al.*, 2009]. (Fault) stresses are then related to (fault) slip as

$$\sigma(t) = -kx - \int_0^t \lambda\sigma(\tau)\, d\tau,$$

where x (meter) is fault slip, t (seconds) is time, σ (Pa) is shear stress magnitude on the fault and k (Pa·m^{-1}) and λ (s^{-1}) are constants. The first right term on the right hand side of the equation determines the instantaneous frictional response to fault slip, with k determining the magnitude of the instantaneous response. The second term determines the relaxation rate of shear stress on the fault and λ is equal to the inverse of the relaxation time. Assuming that fault friction is constant with time gives

$$\sigma + \lambda\sigma t = -kx \quad \text{and if } t\frac{1}{\lambda}: \quad \sigma = -\frac{k}{\lambda}v$$

with fault slip rate v. In steady state, shear stress on the fault is thus proportional and opposite to the fault slip rate. The ratio k/λ ("kinematic fault friction"; $Pa \cdot s \cdot m^{-1}$) determines the mechanical coupling across faults. Typical values of λ and k are on the order of 10^{-11} s^{-1} and 10^5-10^6 Pa·m^{-1}, respectively. This gives a range between $1 \cdot 10^{16}$ and $1 \cdot 10^{17}$ Pas·m^{-1} for the unknown kinematic fault friction. In section 5, we further constrain the kinematic fault friction using (present-day) GPS velocities, maximum compressive stress directions, and focal mechanisms.

Figure 3 shows the (intra-plate) faults in our domain. Motion at faults is a response to model stresses. At intra-plate faults we allow both strike-parallel and down-dip / up-dip slip. Steeply dipping faults like the Septentrional Fault, are allowed only to move in a strike-parallel direction. The southern boundary of the Gonave block (Enriquillo-Plantain-Garden FZ and the Walton fault), which is predominantly strike-slip, is allowed to slip both parallel and down/up-dip the fault plane, because the 12 January 2010 event just north of the Enriquillo-Plantain-Garden FZ indicated a (minor) component of convergence [*Calais et al.*, 2010].

Calculation of uplift rate

In our spherical plane stress models, uplift is derived from the vertical strain ε_{zz} (in the plane stress approximation) given by

$$\varepsilon_{zz} = \frac{\nu(\varepsilon_{xx} + \varepsilon_{yy})}{1-\nu},$$

with ν the Poisson ratio and ε_{xx} and ε_{yy} the horizontal components of the strain tensor. Consistent with our approach of working with a spherical shell, we assume that the strain is constant to a depth of L = 100 km. We also assume that tectonic uplift is slow so that local isostatic equilibrium is maintained. The surface uplift H is then given by

$$H = \frac{\rho_a - \rho_l}{\rho_a - \rho_{air,water}} \varepsilon_{zz} L,$$

with ρ_a (3354 kg.m^{-3}) the density of the asthenosphere, ρ_l (3197 kg.m^{-3}) the average density of the lithosphere, and ρ_{air} the density of air (uplift), and ρ_{water} the density of water (subsidence). The values ρ_a and ρ_l are the weighted average values for the Caribbean region, obtained from the Crust2.0 model [*Bassin et al.*, 2000]. The uplift rate is obtained by taking the time derivative of the uplift.

5. Benchmarking and analysis of present-day models

In this section, we use results of Bahamas Collision and Slab Edge Push driven models for the Present-day to select values for the kinematic fault friction and regional viscosity for the region. Varying these model parameters, we search for values that minimize the misfit to observations.

Observations

Observations of GPS-derived velocities, principal stress axes and focal mechanisms are presented in Figure 4a. We compiled GPS-derived velocities for the northeastern Caribbean region from Calais et al. [2002], DeMets et al. [2000], DeMets and Wiggins-Grandison [2007], Jansma et al. [2000],

López et al. [2006], Mann et al. [2002], and Weber et al. [2001]. To obtain velocities in the same Caribbean reference frame, we first rotate the reported velocities into the ITRF2000 reference frame. Transformation into the Caribbean reference frame is accomplished by the appropriate vectorial addition of the velocity of the Caribbean plate relative to ITRF2000, using the angular velocity vector of 36.3˚N, 98.5˚W, 0.255˚·Myr^{-1} [*DeMets et al.*, 2007]. For multiple reports of site velocities at one station, the reported velocity with the smallest standard deviation is used.

Directions of maximum compressive horizontal stress come from the World Stress Map [WSM, *Heidbach et al.*, 2008]. We only use 'A', 'B' and 'C' -quality measurements, corresponding to 15˚, 20˚ and 25˚ of uncertainty respectively. The majority (24 out of 26) of the measurements are of 'C'-quality.

The focal mechanisms come from the Centroid Moment Tensor (CMT) Catalogue (Available from http://www.globalcmt.org). To assure that only the lithospheric stress is sampled, only events located between 0 and 33 km depth are used. Some of the focal mechanisms have also been used in the compilation of the world stress map; here we also use the orientation of the nodal planes, information that is not available in the world stress map. An estimate of the observed strain rate can be obtained by spatially interpolating the moment tensors using a Gaussian function of distance to the hypocenter, followed by a Kostrov summation [*Kostrov*, 1974]. This gives a strain rate, which is on average $1 \cdot 10^{-3}$ Myr^{-1}. Since not all earthquakes are recorded in the CMT catalogue, and strain rate can also manifest itself aseismically, this is a minimum estimate. The average strain rate for the north Caribbean plate boundary zone as computed by Kreemer [2001] is on the order of $1 \cdot 10^{-2}$ Myr^{-1}. We use a range of $10^{-3} - 10^{-2}$ Myr^{-1} for the observed strain rate.

Comparison with observations

For both scenarios we use observed GPS-derived velocities, principal stress axes and focal mechanisms to tune the unknown domain viscosity and kinematic fault friction. The average difference in direction of the modeled principal axes with the World Stress map (WSM) [*Heidbach et al.*, 2008] is computed following:

$$\Delta\bar{\alpha} = \frac{1}{N_\alpha}\sum_{i=1}^{N_\alpha}\left|\alpha_i^{WSM} - \alpha_i^{model}\right|,$$

where N_α is the number of stress observations, α_i^{WSM} and α_i^{model} are the *i*-th observed and modeled direction of maximum horizontal compression, respectively. The average misfit of modeled velocities with GPS-derived velocities is calculated by:

$$\Delta\bar{v} = \frac{1}{N_v}\sum_{i=1}^{N_v}\sqrt{\left(v_{i,x}^{GPS} - v_{i,x}^{model}\right)^2 + \left(v_{i,y}^{GPS} - v_{i,y}^{model}\right)^2},$$

where N_v is the number of velocity observations, $\left(v_{i,x}^{GPS},\ v_{i,y}^{GPS}\right)$ and $\left(v_{i,x}^{model},\ v_{i,y}^{model}\right)$ are the *i*-th observed and modeled horizontal velocity vectors, respectively. Slip directions on existing fault planes of earthquakes (taken from the Centroid Moment Tensor (CMT) catalogue are calculated following Meijer [1995]. In this approach it is assumed that the fault plane already existed prior to the earthquake and that slip on the fault plane is in the direction of maximum resolved shear stress. Given the modeled stress field we compute the predicted slip direction and compare this with the observed slip direction. We do this for both nodal planes. The fact that there are two nodal planes for any focal mechanism solution is an inherent ambiguity in the data. For the calculation of the average misfit we use the nodal plane that yields the smaller misfit:

$$\Delta\bar{\beta} = \frac{1}{N_\beta}\sum_{i=1}^{N_\beta}\left|\beta_i^{CMT} - \beta_i^{model}\right|,$$

where N_β is the number of focal mechanisms, β_i^{CMT} and β_i^{model} are the *i*-th observed and modeled rake, respectively.

The results of the Bahamas Collision model and the Slab Edge Push model are very similar for optimally selected values of the viscosity and kinematic fault friction (Figure A.1, Table 4). The average misfit of GPS velocities is 3.12 mm·yr^{-1} for the east-west velocity, and 1.72 mm·yr^{-1} for the north-south component. The (average) 95% confidence ellipse of the data has an east-west axis of 2.48 mm·yr^{-1} and north-south axis of 1.71 mm·yr^{-1}. The average misfit of the WSM data is 26.9º whereas the average data uncertainty is 24º. We conclude therefore that the statistical fit of both present-day models to the GPS and WSM observations is acceptable.

Figures 4b and 4c show the sensitivity of the misfit of the Bahamas Collision and Slab Edge Push models to kinematic fault friction and viscosity. The magnitudes of computed velocities and strain rates are most sensitive to the viscosity of the domain. A viscosity of $1 \cdot 10^{23}$ Pa·s gives the smallest misfit for the velocities for both models. This viscosity is identical to the result of Tesauro et al. [2012] for the Caribbean region. A kinematic fault friction of 45 $Pa \cdot s \cdot m^{-1}$ gives the best fit with the observations for both models.

We conclude that both mechanisms explain the present-day observations equally well, i.e., the two scenarios cannot be discriminated on the basis of present-day observations. As a consequence, we can also not constrain the relative contribution of Bahamas Collision and Slab Edge Push to the present-day deformation of the northeastern Caribbean plate boundary zone.

6. Results and analysis of models for 30-2.5 Ma.

Back in time, both scenarios have a diachronous character. In the Slab Edge Push scenario the diachroneity stems from the moving slab edge, which was located east of Puerto Rico from 30 to 25 Ma (Figure 3b, right column). During 25-8 Ma the slab edge passed beneath the Puerto Rico microplate. From 8 Ma to Present the slab edge was active under the Hispaniola microplate. Since around 18 Ma the Bahamas Platform started colliding, first at the plate boundary in the northwest of Puerto Rico, and from around 12 Ma north of Hispaniola (Figure 3b, left column).

Model results

Slab Edge Push results in compression and uplift ahead/west of the location of the slab edge, and in tension and subsidence in the wake of it. Stresses and strain rates would decrease simply with distance from the slab edge were it not for the regional faults that complicate their patterns. As the slab edge migrates beneath varying fault geometries, stress and strain rate distributions do not simply translate (figures A.2-4 and Supplementary movies). Slab Edge Push acts on an area that extends deeper in the north than in the south (figure 2). A uniform traction (per unit area) therefore results in a

higher (line) force in the north than in the south, i.e., the propensity to drive a vertical CCW rotation immediately west of the slab. The extent to which this is expressed in the deformation depends again strongly on the constellation of nearby faults (figure 5). From 30 to 25 Ma, the slab edge was located east of Puerto Rico. As a consequence, the model predicts a relatively small CCW vertical axis rotation rate of ~1°/Myr of the Puerto Rico microplate (Figure 5a). During the following period when the slab edge passes beneath the Puerto Rico microplate (25 to 8 Ma), CCW rotation rates of the Puerto Rico microplate increase to almost 5º/Myr (Figure 5). Shear coupling across the Mona Rift fault drives a small CW rotation of the Hispaniola microplate during this period. When the slab edge migrates beneath the Hispaniola microplate, rotation rates in Puerto Rico decrease to less than 1°/Myr. During this period (8 Ma-Present), vertical axis rotation rates of Hispaniola are predicted to become ~1°/Myr CCW (Figure 5c, d).

Bahamas Collision builds up from 18 Ma. During the pre-collision phase (30-18 Ma), frictional coupling between the North America and Caribbean plates causes stresses, vertical motions and deformation of the northeastern Caribbean plate boundary zone (figures A.2-4 and Supplementary movies). Both the Puerto Rico and Hispaniola microplate show a ~1°/Myr CCW rotation rate (figure 5) in response to this pre-collisional shearing. The imprint of Bahamas Collision becomes noticeable from 12 Ma, when stresses, vertical motions and deformation rates increase, and when the vertical axis rotation rate of Hispaniola becomes ~1.5°/Myr (figure 5).

Comparison of Bahamas Collision and Slab Edge Push models

Both models are characterized by a diachronous evolution from east to west. Slab Edge Push particularly leaves a strong diachronous signature on the resulting strain rate, stress, uplift rate and rotation rate fields . The Slab Edge Push models predict uplift and contraction in front of(west) - and subsidence and extension in the wake of (east) - the slab edge. The magnitudes are much more pronounced than in the Bahamas Collision models. The effects of the slab edge are geographically more widespread and are also felt in the interior of the Caribbean plate. In the Bahamas Collision models

compression (and accompanying uplift) is predominantly confined to the Septentrional fore-arc sliver, while the tectonic regime in Puerto Rico and away from the Septentrional fault in Hispaniola is predominantly (trans) tensional (Figures A.2a-d and A.3a-d). Strain, rotation and uplift rates are more constant with time and only from 12 Ma, when the Bahamas Collision becomes active, rates increase in Hispaniola. In both models strain and uplift rates are high along faults, in particular the Septentrional Fault, but in particular the BAHAMAS models are dominated by along-fault deformation. Differences between the models in the Puerto Rico-Virgin Islands microplate are strong between 25 and 8 Ma, when the slab edge passes beneath this microplate. In the Hispaniola microplate, differences between the two scenarios become stronger after ~8 Ma. (Figures A.2d, A.3d, A.4d and 5d).

Hippolyte [2005] determined principal strain directions in northwest Puerto Rico. During the Eocene, the shortening was north-south directed and the regime was transpressional. Both models fail to reproduce this north-south shortening around 30 Ma (Figures A.2a and A.3a). In south-central Puerto Rico, observed shortening was north(east)-south(west) during the Eocene [*Erikson et al.*, 1990]. Both models predict the maximum compression in this direction (Figures A.2a and A.3a). Observations of uplift and subsidence indicate that the northern coast of Puerto Rico was first characterized by uplift during the Oligocene, followed by shallow Early Miocene carbonate deposition, and Middle Miocene – Pliocene large-scale tilting and subsidence [*Larue et al.*, 1998]. This pattern of uplift followed by subsidence is in better agreement with the Slab Edge Push models. It is not observed in the BAHAMAS models (Figures A.4a,b,c and d).

During the Miocene, principal stresses in northwest Puerto Rico were E-W extensional [*Hippolyte et al.*, 2005], which is also observed in the Slab Edge Push models (Figures A.2b,c A.3b,c). However, it should be noted that the observations are local and possibly reflect the influence of dynamic topography caused by sinking density anomalies associated with the subducting Puerto Rico slab. Observed stress directions in Hispaniola indicate northeast-southwest contraction during the Neogene, and in particular the Pliocene [*de Zoeten and Mann*, 1991; *Heubeck and Mann*, 1991]. This is reproduced by

both models (Figures A.2d and A.3d). Hispaniola is characterized by several tectonic phases, mainly compression and uplift, in particular during the Pliocene [*de Zoeten and Mann*, 1991; *Heubeck and Mann*, 1991]. Both the Slab Edge Push and BAHAMAS models have a pattern of both uplift and subsidence in Hispaniola, dominated by uplift since 10 Ma.

Thrusting at the Muertos Trough might have started during the large CCW-rotation of Puerto Rico [*Masson and Scanlon*, 1991] around 11 Ma. The amount of subduction is unclear, but based on the Wadati-Benioff Zone and tomography it amounts to no more than 150 km [*Dolan et al.*, 1998; *van Benthem et al.*, 2013]. At least 40 km of convergence has been estimated at 68.5°W [*Ladd et al.*, 1977]. This gives an average convergence rate of 3.6-13.6 mm·yr^{-1} during the last 11 Myr, although GPS-derived velocities suggest much lower values at present. The nature of the Anegada fault zone is not very well established, but is most likely transtensional [*Jany et al.*, 1990; *Raussen et al.*, 2013]. The Virgin Islands basin, located in this fault zone, 20 km wide and 75 km long is a result of this transtension, suggesting a minimum of 20 km of extension [*Raussen et al.*, 2013]. The model of Masson and Scanlon [1991], where the Puerto Rico-Virgin Islands microplate experienced a large amount of Miocene rotation, dictates that the amount of extension in the Anegada fault is comparable to the amount of convergence at the Muertos Trough (40-150 km). Extension in the Mona Rift is estimated to be at least 0.1 mm·yr^{-1} during the Late Oligocene-Early Miocene, increasing to at least 0.4 mm·yr^{-1} since the Late Miocene [*Mondziel et al.*, 2010]. This leads to a minimum estimate of 6.1 km of extension in total. Lateral offset are not reported for this fault. Calmus [1983] estimated around 30-50 km of total fault offset for the Enriquillo-Plantain-Garden fault zone since the Cretaceous.

The average fault slip predicted by the models is listed in Table 5. We find that both models give estimates of fault slip for the Muertos Trough, Enriquillo-Plantain-Garden Fault and Anegada Fault zones that are a factor of ~two too high. This could either indicate that the fault zones have been active for a shorter time than modeled, that not all fault displacement has been mapped or that fault friction is higher than assumed in this study. Estimates for the Mona Rift are substantially too high, by a factor of approximately 9 to 19. This probably reflects the fact that Mondziel et al. [2010] only measured the extension and did not take strike-slip motion into account. Finally for the Septentrional fault

zone a Holocene slip rate of 9 ± 3 mm·yr^{-1} has been measured [*Calais et al.*, 2002; *Prentice et al.*, 2003]. Both models give values of around 5 mm·yr^{-1} lower than observations indicate. Apparently the total fault slip resistance for this fault, a combination of visco-elastic deformation along the fault and the imposed kinematic fault friction, is too high in the models. However, as explained earlier, we chose to use uniform parameters throughout the model, although this implies individual misfits, such as at the Septentrional fault zone.

The intra-plate faults effectively decouple the microplates from each other. This implies that the effects of the Slab Edge Push or Bahamas Collision are confined to the microplate it is acting on, and are not felt in a neighboring microplate. This can be observed in the distribution of the strain rate, uplift rate and rotation rates (Figures A.2, A.4, and 5). This localization of the deformation to a microplate should be recognizable in geology. If indications for such localization are absent, faults in that region probably had very high fault friction or were not active yet. The localization emphasizes the diachronous signature of the Slab Edge Push scenario.

One feature of the tectonic reconstruction of Pindell and Kennan [2009] is that approximately 50% of the relative motion between the North America and Caribbean plates was accommodated at faults south of the Greater Antilles. Possibly the slab edge forced the Greater Antilles to partly move along with the North American plate, decreasing sinistral relative plate motion here. When examining the fault slip it is indeed observed that the fault slip increases on the southern faults for the Slab Edge Push models.

Reid et al. [1991] concluded that Puerto Rico rotated 6.5º CW from the late Oligocene (27 Ma) to Early Miocene (22 Ma). This was followed by 5.5º CCW rotation from the Early Miocene to Middle Miocene (11 Ma), 24º CCW rotation during the Middle Miocene–Pliocene, and 1.7º CCW rotation form the Pliocene until Present [*Reid et al.*, 1991]. At present there are no indications for active rotation [*Jansma et al.*, 2000]. Figure 6 compares the observed rotation of Puerto Rico with the modeled rotations of Puerto Rico. The observations in table 2 of Reid et al. (1991) give the total rotations since 27, 22, 11 and 4.5 Ma, plus their 95% confidence intervals. To calculate the rotation during an interval, we took into account the 95% uncertainties at both the start and the end of the interval. Thus the plotted uncertainties of the observed rotations are 90% confidence contours. We calculated the ro-

tations during the same time intervals for all line force sets in Table 1 for both the Slab Edge Push and Bahamas Collision models. Figure 6 shows that the Bahamas Collision models predict rotations that are consistently too low in the period 11-4.5 Ma. Some of the Slab Edge Push models do predict higher rotations during this period, but the expected rotation is too high for these particular models during the period 22-11 Ma.

The Slab Edge Push models better account for observed stresses and uplift/subsidence patterns than the Bahamas Collision models. The total fault slip is higher than observed in both scenarios. The Slab Edge Push models reproduce a pulse of Miocene CCW rotation in Puerto Rico. The Bahamas Collision models produce rotation rates that are constant with time and are less than $1^{o}\cdot Myr^{-1}$. None of the models thus reproduces the observed rotation at all intervals. We therefore proceed to investigate combinations of the two scenarios.

Combined models for force set TSUC5

We expect both mechanisms to contribute to the deformation of the northeastern Caribbean plate boundary zone. Therefore we consider linear combinations of the two end member models with the idea to constrain their relative contribution. An important point in the definition of the combined models is that the total torque contribution should be the same as the torque $\mathbf{T}_C$ that Van Benthem and Govers (2010) established for the Bahamas Collision related forces on the plate boundary segment involved (see Table 3 for list of mathematical symbols and physical units of forces and derived quantities) . Linear combinations of a fraction *f* of the line force by the Slab Edge Push $\mathbf{F}_{\text{sep}}$ and a fraction (1-*f*) of the line force by the Bahamas Collision $\mathbf{F}_{\text{bah}}$ obey:

$$\int_{L_{sep}} \mathbf{r} \times f\mathbf{F}_{\text{sep}} dl + \int_{L_{bah}} \mathbf{r} \times (1-f)\mathbf{F}_{\text{bah}} dl = \mathbf{T}\text{c}$$

where L_{sep} represents the length of the horizontal line where the line force acts that corresponds to the Slab Edge Push, and L_{bah} the length of the trench where the Bahamas Platform collides. Thus

combining the two end member models yields a range of models from one where the contribution by Slab Edge Push is zero and Bahamas Collision maximal (*f*=0), to a model with maximal Slab Edge Push and the Bahamas Collision zero (*f*=1). In this last case, there still is plate boundary friction acting along the North Caribbean margin. As discussed in section 5, the calibration parameters viscosity and kinematic fault friction are equal in both end-member scenarios. The same applies for the linear combinations and we adopt the same values for the viscosity and kinematic fault friction.

Figure 7a summarizes the results for the linear combinations of $\mathbf{F}_{\text{sep}}$ and $\mathbf{F}_{\text{bah}}$. The modeled rotation of Puerto Rico is plotted as function of σ_{sep}, the magnitude of the traction acting on the contact surface between the slab edge and the Caribbean plate (red area in Figure 2). The direction of $\boldsymbol{\sigma}_{\text{sep}}$ is kept constant, throughout the modeling, into the direction of the plate motion of North America relative to the Caribbean. The total block rotation of Puerto Rico increases near-linearly with σ_{sep}. This is a direct result from the fact that the slab edge push was the main force acting on Puerto Rico between 25 and 8 Ma. In models without Slab Edge Push (*f*=0), the rotation of Puerto Rico results from the combination of Bahamas Collision on the westernmost part of Puerto Rico between 18 and 12 Ma and plate boundary friction. For the force model that we consider here (TSUC5), the observed rotation of Puerto Rico including its error margins is reproduced for a σ_{sep} between 21.80 and 51.2 Mpa (f=1). σ_{bah} ranges then between 0.46 (f=1) and 3.51 MPa. The corresponding average magnitudes of the line forces range between 1.09 to 2.56 TN/m ($\hat{F}_{sep}$) and between 0.09 to 0.70 TN/m ($\hat{F}_{bah}$).

Linear combinations for other line force sets

Thus far we presented evaluations of the Slab Edge Push and Bahamas Collision based on the line force set TSUC5 of Van Benthem and Govers (2010). Here we construct linear combinations of the two drivers for alternative force sets (Table 1). Figure 7b shows the total rotation resulting from the combined models for all the line force sets as function of σ_{sep}, compared with the observed rota-

tion.Line force sets with R=1 have no excess traction related to Bahamas Collision. As explained in the "Boundary conditions for the Present-day models" section, this means the Slab Edge Push is also zero for these force sets. None of the models that are based on these force sets reproduce the observed 31° rotation. We conclude that these force sets are unrealistic and that an extra traction (either Bahamas Collision or Slab Edge Push) is needed along the northeastern Caribbean plate boundary zone.

For f = 0, i.e. the Slab Edge Push is 0, the amount of rotation varies with the different force sets (Figure 7b), although the Slab Edge push is the same. This is because Bahamas Collision and Puerto Rico Trench tractions are different for these force sets. The figure shows that models with higher R require higher σ_{sep} to reproduce the observed rotation. This can be understood from the fact that high-R force sets have lower plate boundary friction (Table 2), which thus contributes little to the rotation of Puerto Rico. The observed rotation of Puerto Rico is reproduced for those traction magnitudes that are in the shaded areas in figure 7b: 11.21 MPa (TSUC3) $\leq \sigma_{sep} \leq$ 102.13 MPa (TSUC10) (equivalent with 0.55 TN/m $\leq \hat{F}_{sep} \leq$ = 5.01 TN/m) and 0.61 MPa $\leq \sigma_{bah} \leq$ 12.38 MPa (equivalent with 0.12 TN/m $\leq \hat{F}_{bah} \leq$ = 2.48 TN/m). Similar to what we concluded previously for force set TSUC5, our evaluation of all possible force sets thus shows that combined forcing by Slab Edge Push and Bahamas Collision successfully reproduces the observed rotation of Puerto Rico.

The torques corresponding to Slab Edge Push and Bahamas Collision represent integral contributions to the mechanical stability and motion of the Caribbean plate as a whole. For the successful models in our study, the torque magnitude corresponding to Bahamas Collision ranges from $1.06 \cdot 10^{24}$ to $15.93 \cdot 10^{24}$ Nm and the torque from Slab Edge Push from $2.14 \cdot 10^{24}$ to $19.62 \cdot 10^{24}$ Nm. These magnitudes are very similar and lead us to the conclusion that the contributions of the Bahamas Collision and Slab Edge Push to the motion of the Caribbean plate are roughly equal.

Regional variations in tractions cause intra-plate stresses that drive deformation. Due to the map view nature of our models, the propensity to cause deformation is represented by depth-integrated tractions, i.e., by line forces. The average line force magnitude corresponding to Slab Edge Push comes out to be roughly twice as large as the line force magnitude from Bahamas Collision:

0.55 TN/m $\leq \hat{F}_{sep} \leq$ = 5.01 TN/m and 0.12 TN/m $\leq \hat{F}_{bah} \leq$ = 2.48 TN/m. We thus conclude that the Slab Edge Push is the dominant driver of observed deformation and fragmentation along the north-eastern Caribbean plate boundary zone.

7. Conclusions

Push by the westward migrating Puerto Rico slab edge causes deformation in the northeastern Caribbean plate boundary zone. This driver acts in addition to collision of the Bahamas Platform. The relative contributions of this Slab Edge Push and Bahamas Collision to the present-day deformation cannot be resolved from observations because both mechanisms cause similar deformation. Observations for the period since the Late Oligocene do allow us to identify the contributions of the two drivers: a combination of Slab Edge Push and Bahamas Collision, with push dominating over collision, best explains the deformation of the northeastern Caribbean plate boundary zone.

8. Acknowledgements

We thank an anonymous reviewer, Reinoud Vissers, Giovanni Bertotti and Lorcan Kennan for thoughtful comments that helped us to improve the manuscript. SvB was supported by ALW/NWO project 816.01.008 “How plate tearing and slabs drive reorganization of the north Caribbean plate boundary”.

9. Appendix:

Additional model results for the present-day

Figure A.1 shows the results for the best fitting BAHAMAS0 and SEP0 models. In both models the highest strain rates are found on the Hispaniola block (Figure A.1a). In BAHAMAS0 this is a result of the Bahamas Collision force acting on this block and in the SEP0 model this is a result of the Slab Edge Push that is also acting on this block (Figure 3). The highest strain rates are found along the Septentrional fault zone, which is caused by the restriction on fault-perpendicular slip here. Away from the plate boundary zone principal stress axes are roughly northeast-southwest directed in both models, reflecting the relative plate motions in the area. SEP0 shows extension to the east (in the wake) of the indenting slab edge, and shortening at the Hispaniola block to the west. BAHAMAS0 also shows shortening in the Hispaniola-block, whereas to the east the regime is trans-tensional. The bending and deformation of the Septentrional fore-arc sliver results in both local tension (resulting in extension) and compression (contraction). The distribution of the strain rate indicates that the intra-plate faults mechanically decouple the microplates, i.e. high strain rates caused by the Slab Edge Push or the Bahamas Collision are confined to the Hispaniola block.

Figure A.1b shows uplift rate and horizontal velocities of both models. They are characterized by uplift in Hispaniola, although the irregular geometry of the faults and plate bending in the horizontal plane locally causes subsidence. Puerto Rico is characterized by subsidence. Velocities in the Hispaniola and Puerto Rico - Virgin Islands microplates for SEP0 are more to the south than for BAHAMAS0, and more in line with the relative motion between the North America and Caribbean plates in this plate boundary region. This suggests that the slab edge, with its relative direction almost perpendicular to the line of application, pushes the motion of the microplate. The Bahamas Platform, which collides in a direction highly oblique to the segment of the plate boundary it is acting on, rather shears and deforms the Hispaniola block, causing deviations from the direction of North America – Caribbean relative plate motion.

Figure A.1c shows the rotation rate around a vertical axis, $\dot{\omega}_{xy}$, and the differential fault velocities. Both models have counterclockwise (CCW) rotations in Hispaniola. Rotation of Puerto Rico is CCW in the SEP0 model and almost absent in the BAHAMAS0 model. In the stable Caribbean or North America plates, rotations are close to zero. Fault slip is very similar for both models, with oblique convergence along the main plate boundary, extension in the Mona Rift and Anageda fault zone, and transpressional for the Enriquillo-Plantain-Garden fault, Muertos Trough and Hispaniola fault.

The Bahamas Collision causes less deformation than the Slab Edge Push. This is partly because the line force for the Bahamas Collision is distributed over a longer plate boundary segment than the line force for the Slab Edge Push, and partly because the Septentrional fault zone decouples part of the Bahamas Collision force from the interior of the Hispaniola microplate. It is also interesting to note that the Slab Edge Push model predicts uplift for the interior of the Caribbean plate, roughly at the location of the present-day Beata ridge, whereas the consequences of the Bahamas Collision are more limited.

Additional model results for 30-2.5 Ma

Figures A.2-4 show the results for both scenarios from 30 to 2.5 Ma. Supplementary movies are useful to appreciate the evolution of both models.

The Slab Edge Push models predict a transpressional regime and uplift in Puerto Rico from 30 to 25 Ma, when the slab edge was located east of Puerto Rico. Hispaniola is characterized by uplift and transpression along faults, in particular the Septentrional fault zone (Figures A.2a and A.3a). Maximum compression in Puerto Rico is northeast-southwest directed and in Hispaniola it ranges from northwest-southeast to northeast-southwest (Figure A.2a). During the period that the slab edge passes beneath the Puerto Rico microplate (25 to 8 Ma), uplift and compression in Puerto Rico change to tension, or trans-tension, and subsidence (Figures A.3b, c and A.4b, c). Around 8 Ma the slab edge migrates beneath the Hispaniola microplate. This increases strain rates and uplift rates here, while strain and uplift rates decrease in Puerto Rico (Figures A.2c, d and A.4c, d). The stress regime in His-

paniola becomes more transpressional (Figure A.3c, d).

The Bahamas Collision models show (trans)tension and subsidence in Puerto Rico from 30 to 18 Ma, (Figures A.3a, b and A.4a, b). During this pre-collisional phase, deformation of the northeastern Caribbean plate boundary zone is entirely driven by friction. The directions of maximum compression are northeast-southwest directed (Figure A.2a, b). In Hispaniola there are regions with transtension and subsidence and other regions with transpression and uplift. This is particularly the case along the Septentrional fault zone. The direction of maximum compression varies from east-west to north-south (Figures A.2a-b, A.3a-b and A.4a-b). Around 18 Ma, the Bahamas Platform started colliding, first in the east of Puerto Rico and from ~12 Ma in Hispaniola. Initially the contact surface between the Bahamas Platform and the Caribbean plate was relatively small. In the BAHAMAS models differences with respect to the pre-collisional phase are therefore relatively small initially (Figures A.2c, A.3c, A.4c, 5c). From 12 Ma the Bahamas Collision becomes active in the east of Hispaniola, resulting in an increase of strain, uplift and rotation rates here.

Timing of Rotation Rate

We calculate the average rotation rates during the time intervals from 27 to 22 Ma, 22 to 11 Ma, 11 to 4.5 Ma and 4.5 Ma to Present. This can be compared with modeled rotation rates during the same intervals, presented in Figure A.5 The models show a pulse in rotation rate for Puerto Rico between 25 and 8 Ma. This contrasts with the observed pulse in CCW rotation, that lies between 11 and 4.5 Ma. This outcome might be resolved in two ways: Either the slab edge at Present is located further east than assumed in the models, or the relative westward motion of the North America plate (and the slab edge) with respect to the Caribbean was higher than assumed in the models. However, both the present-day slab edge and the relative plate motion are well established by geological observations.

References

Ali, S. T., A. M. Freed, E. Calais, D. M. Manaker, and W. R. McCann (2008), Coulomb stress evolution in Northeastern Caribbean over the past 250 years due to coseismic, postseismic and interseismic deformation, *Geophys. J. Int.*, *174*(3), 904-918.

Álvarez-Gómez, J. A., P. T. Meijer, J. J. Martínez-Díaz, and R. Capote (2008), Constraints from finite element modeling on the active tectonics of northern Central America and the Middle America Trench, *Tectonics*, doi: 10.1029/2007TC002162.

Bassin, C., G. Laske, and G. Masters (2000), The Current Limits of Resolution for Surface Wave Tomography in North America, *EOS, T. Am. Geoph. U.*, *81*, F897.

Byrne, D. B., G. Suarez, and W. R. McCann (1985), Muertos Trough subduction - microplate tectonics in the northern Caribbean?, *Nature*, *317*, 420-421.

Calais, E., J. Perrot, and B. Mercier de Lépinay (1998), Strike-slip tectonics and seismicity along the northern Caribbean plate boundary from Cuba to Hispaniola, in *Active Strike-Slip and Collisional Tectonics of the Northern Caribbean Plate Boundary Zone*,, edited by J. F. Dolan and P. Mann, pp. 125-141, Geological Society of America Special Paper 326, Boulder, CO.

Calais, E., Y. Mazabraud, B. M. deLepinay, P. Mann, G. Mattioli, and P. Jansma (2002), Strain partitioning and fault slip rates in the northeastern Caribbean from GPS measurements, *Geophys. Res. Lett.*, *29*(18), 1856-1860.

Calais, E., A. Freed, G. Mattioli, F. Amelung, S. Jonsson, P. Jansma, S.-H. Hong, T. Dixon, C. Prepetit, and R. Momplaisir (2010), Transpressional rupture of an unmapped fault during the 2010 Haiti earthquake, *Nature Geosc.*, *3*(11), 794-799.

Calmus, T. (1983), Contribution to the Geologic Study of the Macay Massif (Southwest Haiti, Greater Antilles): 'Sa place'' of the evolution of the Northern Caribbean Orogeny (Contribution à l'étude géologique du Massif du Macaya (sud-ouest d'Haiti, Grandes Antilles): Sa place dans l'évolution de l'orogène Nord-Caraïbe), Ph. D. thesis, 163 pp, Université Pierre et Marie Curie, Paris, France.

de Zoeten, R., and P. Mann (1991), Structural Geology and Cenozoic Tectonic History of the Central Cordillera Septentrional, Dominican-Republic, in *Geologic and Tectonic Development of the North America-Caribbean Plate Boundary in Hispaniola*, edited by P. Mann, G. Draper and J. F. Lewis, pp. 265-279, Geological Society of America Special Paper 262.

DeMets, C., and M. D. Wiggins-Grandison (2007), Deformation of Jamaica and motion of the Gonave microplate from GPS and seismic data, *Geophys. J. Int.*, *168*(1), 362-378.

DeMets, C., G. Mattioli, P. Jansma, R. Rogers, C. Tenorio, and H. Turner (2007), Present motion and deformation of the Caribbean plate: Constraints from new GPS geodetic measurements from Honduras and Nicaragua, in *Geologic and Tectonic development of the Caribbean plate boundary in northern Central America*, edited by P. Mann, pp. 21-36, Geological Society of America Special Papers 428, Boulder, CO, USA,.

DeMets, C., P. E. Jansma, G. S. Mattioli, T. H. Dixon, F. Farina, R. Bilham, E. Calais, and P. Mann (2000), GPS geodetic constraints on Caribbean-North America plate motion, *Geophys. Res. Lett.*, *27*(3), 437-440.

Dillon, W. P., J. A. Austin, Jr., K. M. Scanlon, N. T. Edgar, and L. M. Parson (1992), Accretionary margin of north-western Hispaniola: Morphology, structure, and development of the northern Caribbean plate boundary, *Mar. Petrol. Geol.*, *9*, 70-88.

Dolan, J. F., and D. J. Wald (1998), The 1943-1953 north-central Caribbean earthquakes: Ac-

tive tectonic setting, seismic hazards, and implications for Caribbean-North American plate motions, in *Active Strike-Slip and Collisional Tectonics of the Northern Caribbean Plate Boundary Zone*, edited by J. F. Dolan and P. Mann, pp. 143-169, Geological Society of America Special Paper 326, Boulder, CO.

Dolan, J. F., H. T. Mullins, and D. J. Wald (1998), Active tectonics of the north-central Caribbean: Oblique collision, strain partitioning, and opposing subducted slabs, in *Active Strike-Slip and Collisional Tectonics of the Northern Caribbean Plate Boundary Zone*, edited by J. F. Dolan and P. Mann, pp. 1-61, Geological Society of America Special Paper 326, Boulder, CO.

Erikson, J. P., J. L. Pindell, and D. K. Larue (1990), Mid-Eocene-early Oligocene sinistral transcurrent faulting in Puerto Rico associated with formation of the northern Caribbean Plate boundary zone, *J. Geol.*, *98*(3), 365-384.

French, C. D., and C. J. Schenk (2004), Map Showing Geology, Oil and Gas Fields, and Geologic Provinces of the Caribbean Region, *Open File Rep. 97-470-K*, U.S.G.S., Reston, USA.

Furlong, K. P., and R. Govers (1999), Ephemeral crustal thickening at a triple junction:The Mendocino crustal conveyor, *Geology*, *27*(2), 127-130.

Grindlay, N. R., P. Paul Mann, J. F. Dolan, and J.-P. van Gestel (2005), Neotectonics and subsidence of the northern Puerto Rico–Virgin Islands margin in response to the oblique subduction of high-standing ridges, in *Active Tectonics and Seismic Hazards of Puerto Rico, the Virgin Islands, and Offshore Areas*, edited by P. Mann, pp. 31–60, Geological Society of America Special Paper 385, Boulder, CO, USA.

Heidbach, O., M. Tingay, A. Barth, J. Reinecker, D. Kurfeß, and B. Müller (2008), The 2008 release of the World Stress Map (available online at www.world-stress-map.org) edited.

Heubeck, C., and P. Mann (1991), Structural geology and Cenozoic tectonic history of the southeastern termination of the Cordillera Central, Dominican-Republic, in *Geologic and Tectonic Development of the North America-Caribbean Plate Boundary in Hispaniola*, edited by P. Mann, G. Draper and J. F. Lewis, pp. 315-336, Geological Society of America Special Paper 262, Boulder, CO.

Hippolyte, J.-C., P. Mann, and N. R. Grindlay (2005), Geologic evidence for the prolongation of active normal faults of the Mona rift into northwestern Puerto Rico, in *Active Tectonics and Seismic Hazards of Puerto Rico, the Virgin Islands, and Offshore Areas*, edited by P. Mann, pp. 161–171, Geological Society of America Special Paper 385.

Jansma, P., A. Lopez, G. Mattioli, C. DeMets, T. Dixon, P. Mann, and E. Calais (2000), Microplate tectonics in the northeastern Caribbean as constrained by Global Positioning (GPS) geodesy, *Tectonics*, *19*, 1021-1037.

Jany, I., K. M. Scanlon, and A. Mauffret (1990), Geological interpretation of combined Seabeam, GLORIA and seismic data from Anegada Passage (Virgin Islands, North Caribbean), *Mar. Geophys. Res.*, *12*(3), 173-196.

Kostrov, V. (1974), Seismic moment and energy of earthquakes, and seismic flow of rock, *Phys. Sol. Earth*, *1*, 13-21.

Kreemer, C. W. (2001), A Global Strain Rate Model, PhD thesis, 170 pp, State University of New York at Stony Brook, Stony Brook, NY.

Ladd, J., J. Worzel, and J. Watkins (1977), Multifold seismic reflection records from the northern Venezuelan Basin and the northern slope of the Muertos Trench, in *Island Arcs, Deep Sea Trenches, and Back-arc Basins*, edited by M. Talwani and W. C. Pitman, III, pp. 41- 56, American Geophysical Union 1, Washington, D.C.

Larue, D. K., R. Torrini, Jr., A. L. Smith, J. Joyce, E. G. Lidiak, and D. K. Larue (1998), North Coast Tertiary basin of Puerto Rico; from arc basin to carbonate platform to

arc-massif slope, in *Tectonics and geochemistry of the northeastern Caribbean*, edited by E. G. Lidiak and D. K. Larue, pp. 155-176 Special Paper 322, Boulder, CO, USA.

Leroy, S., A. Mauffret, P. Patriat, and B. M. de Lepinay (2000), An alternative interpretation of the Cayman trough evolution from a reidentification of magnetic anomalies, *Geophys. J. Int.*, *141*(3), 539-557.

López, A., S. Stein, T. Dixon, G. Sella, E. Calais, P. Jansma, J. Weber, and P. LaFemina (2006), Is There a Northern Lesser Antilles Forearc Block?, *Geophys. Res. Lett.*, *33*, doi: 10.1029/2005GL025293.

Manaker, D. M., E. Calais, A. M. Freed, S. Ali, P. Przybylski, G. Mattioli, P. Jansma, C. Prépetit, and J. B. de Chabalier (2008), Interseismic Plate coupling and strain partitioning in the Northeastern Caribbean, *Geophys. J. Int.*, *174*(3), 889-903.

Mann, P., E. Calais, J. C. Ruegg, C. DeMets, P. E. Jansma, and G. S. Mattioli (2002), Oblique collision in the northeastern Caribbean from GPS measurements and geological observations *Tectonics*, *21*(6), 1057-1083.

Masson, D. G., and K. M. Scanlon (1991), The neotectonic setting of Puerto Rico, *Geol. Soc, Am. Bull.*, *103*(1), 144-154.

Meighan, H. E., J. Pulliam, t. Brink, U., and A. M. López-Venegas (2013), Seismic evidence for a slab tear at the Puerto Rico Trench, *Journal of Geophysical Research-Solid Earth*, *118*(6), 2915-2923, doi: 10.1002/jgrb.50227.

Meijer, P. T. (1995), Dynamics of active continental margins: the Andes and the Aegean region, Geologica Ultraiectina (Ph.D. thesis Utrecht University), 130, 218 pp, Utrecht, the Netherlands.

Melosh, H. J., and C. A. Williams (1989), Mechanics of graben formation in crustal rocks: a finite elemenent analysis, *J. Geophs. Res.*, *94*, 13961-13973.

Molnar, P., and L. R. Sykes (1969), Tectonics of the Caribbean and middle America regions from focal mechanisms and seismicity, *Geol. Soc, Am. Bull.*, *80*, 1639-1684.

Mondziel, S., N. Grindlay, P. Mann, A. Escalona, and L. Abrams (2010), Morphology, structure, and tectonic evolution of the Mona canyon (northern Mona passage) from multibeam bathymetry, side-scan sonar, and seismic reflection profiles, *Tectonics*, *29*(2), TC2003, doi: 10.1029/2008tc002441.

Müller, R. D., J.-Y. Royer, S. C. Cande, W. R. Roest, and S. Maschenkov (1999), New constraints on the Late Cretaceous/Tertiary plate tectonic evolution of the Caribbean, in *Caribbean Basins*, edited by P. Mann, pp. 33-59, Elsevier Science B.V. 4, Amsterdam, The Netherlands.

Negredo, A. M., I. Jiménez-Munt, and A. Villaseñor (2004), Evidence for eastward mantle flow beneath the Caribbean plate from neotectonic modeling, *Geophys. Res. Lett.*, *31*(6), L06615, doi: 10.1029/2003GL019315.

Pardo, G. (1975), Geology of Cuba, in *The Gulf of Mexico and the Caribbean*, edited by A. E. Nairn and F. G. Stehli, pp. 553-615, Plenum Press 3, New York.

Pindell, J. L., and L. Kennan (2009), Tectonic evolution of the Gulf of Mexico, Caribbean and northern South America in the mantle reference frame: an update, in *The Origin and Evolution of the Caribbean Plate*, edited by K. James, M. A. Lorente and J. L. Pindell, pp. 1-55, Geological Society Special Publication 328, London, UK.

Plattner, C., R. Malservisi, and R. Gover (2009), On the plate boundary forces that drive and resist the Baja California motion, *Geology*, *37*(4), 359-362.

Prentice, C. S., P. Mann, L. R. Peña, and G. Burr (2003), Slip rate and earthquake recurrence along the central Septentrional fault, North American-Caribbean plate boundary, Dominican Republic, *J. Geophys. Res.*, *108*(B3), 2149-2166.

Raussen, S., H. Lykke-Andersen, and A. Kuijpers (2013), Tectonics of the Virgin Islands Basin, north eastern Caribbean, *Terra Nova*, *25*(3), 252-257.

Reid, J., P. Plumley, and J. Schellekens (1991), Paleomagnetic evidence for late Miocene counterclockwise rotation of north coast carbonate sequence, Puerto Rico, *Geophys. Res. Lett.*, *18*, 565-568.

Richardson, R. M., and L. M. Reding (1991), North American Plate Dynamics, *J. Geophys. Res.*, *96*(B7), 12201-12223.

Rosencrantz, E., and P. Mann (1991), SeaMARC II mapping of transform faults in the Cayman trough, *Geology*, *19*, 690-693.

ten Brink, U. S., and A. M. López-Venegas (2012), Plate interaction in the NE Caribbean subduction zone from continuous GPS observations, *Geophys. Res. Lett.*, *39*(10), doi: 10.1029/2012gl051485.

Tesauro, M., M. K. Kaban, and S. A. P. L. Cloetingh (2012), Global strength and elastic thickness of the lithosphere, *Glob. Planet. Change*, *90-91*, 51-57.

Turcotte, D. L., and G. Schubert (2002), *Geodynamics, second edition*, 456 pp., Cambridge University Press, Cambridge, England.

van Benthem, S. A. C., and R. Govers (2010), The Caribbean plate: Pulled, pushed, or dragged?, *J. Geophys. Res.*, *115*(B10), B10409, doi: 10.1029/2009jb006950.

van Benthem, S. A. C., R. Govers, W. Spakman, and M. J. R. Wortel (2013), Tectonic evolution and the mantle structure under the Caribbean region, *J. Geophys. Res.*, *118*(6), 3019-3036, doi: 10.1002/jgrb.50235.

Vening Meinesz, F. A., J. H. F. Umbgrove, and P. H. Kuenen (1934), *Gravity expeditions at sea 1923–1932, part 2*, 139 pp., Netherlands Geodetic Commission, Delft.

Vincenz, S. A., and S. N. Dasgupta (1978), Paleomagnetic study of some Cretaceous and Tertiary rocks on Hispaniola, *Pure Appl. Chem.*, *116*, 1200-1210.

Weber, J. C., T. H. Dixon, C. DeMets, W. B. Ambeh, P. Jansma, G. Mattioli, J. Saleh, G. Sella, R. Bilham, and O. Perez (2001), GPS estimate of relative motion between the Caribbean and South American plates, and geologic implications for Trinidad and Venezuela, *Geology*, *29*(1), 75-78.

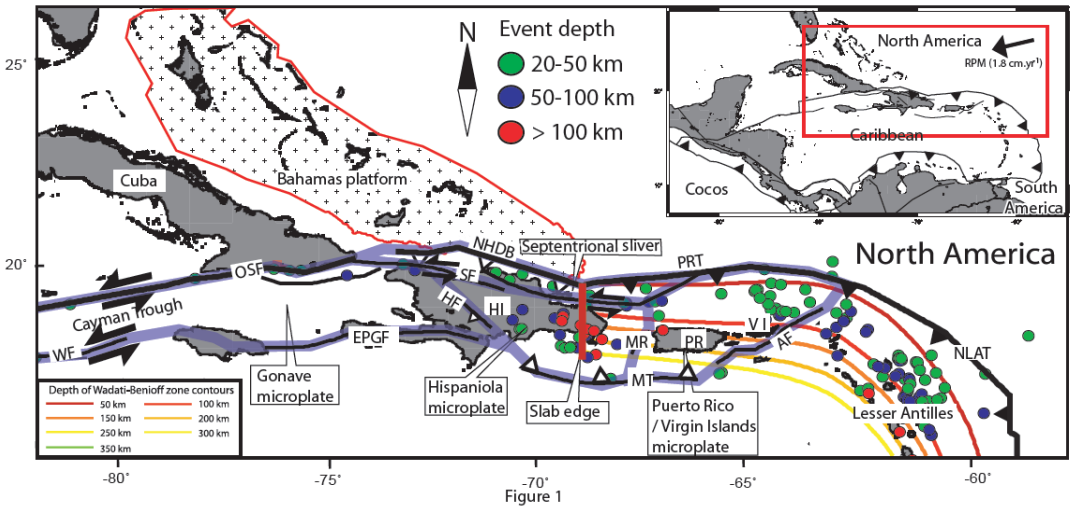

Figure 1

Figure 1

Present-day tectonics of the northeastern Caribbean plate. The inset on the top-right shows the Caribbean plate and surrounding plates, the red box here indicates the domain of the main figure. Bold black lines denote plate boundaries and major faults. Red lines denote major tectonic features mentioned in the text. The Bahamas carbonate platform is indicated by the cross-pattern and the red line. Colored lines show the top of the slab 50-350 km depth [*Gudmundsson & Sambridge, 1998*]. The present-day location of the slab edge is indicated by the thick red line. Regional microplates are bounded by transparent purple lines. Dots denote epicenters deeper than 20 km, taken from the Centroid Moment Tensor (CMT) catalogue (1976 to 2012). Color denotes hypocenter depth. Abbreviations: AF: Anageda Fault; AR: Aves Ridge; EPGF: Enriquillo-Plantain-Garden Fault; HF: Hispaniola Fault; HI: Hispaniola; MR: Mona Rift; MT: Muertos Trough; NHDB: North Hispaniola Deformed Belt; NLAT: Northern Lesser Antilles Trench; OSF: Oriente-Swan Fault; PR: Puerto Rico; PRT: Puerto Rico Trench; SF: Septentrional Fault; VI: Virgin Islands; WF: Walton Fault.

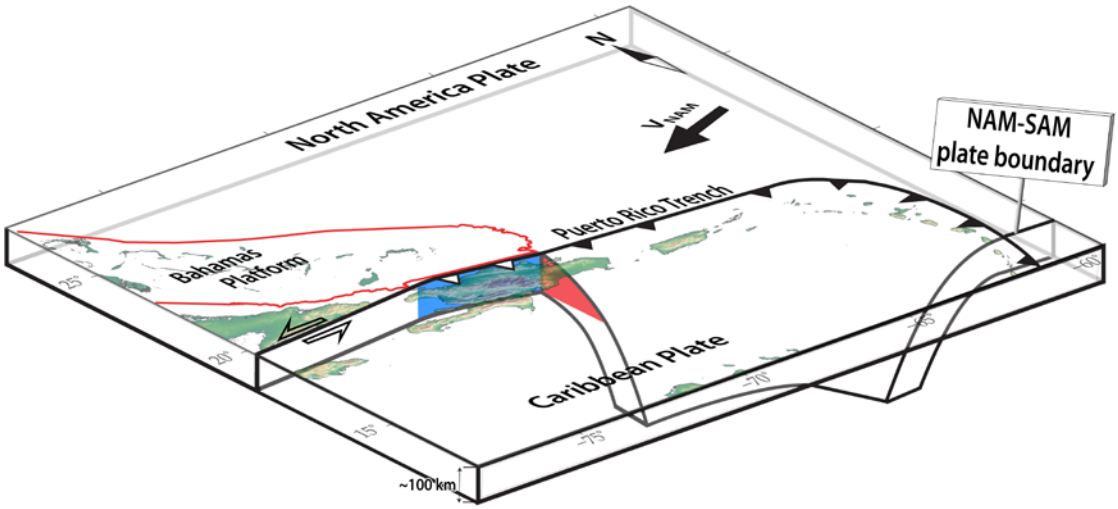

Figure 2

Schematic representation of the northeastern Caribbean plate boundary and the underlying slab structure. The viewpoint is from the southwest. The arrows indicate the direction of relative motion of the North America plate with respect to the Caribbean plate. Relative motion between the Caribbean and North America plates is sinistral with a minor convergent component. The blue area denotes the contact area where the obliquely converging Bahamas Platform (located on the North America plate) pushes against the Caribbean plate. The red area denotes the area where the westward (with a minor component of convergence) moving North America slab edge pushes against the Caribbean plate. The plate boundary between the North America and South America plates is indicated by NAM-SAM plate boundary (van Benthem et al., 2013).

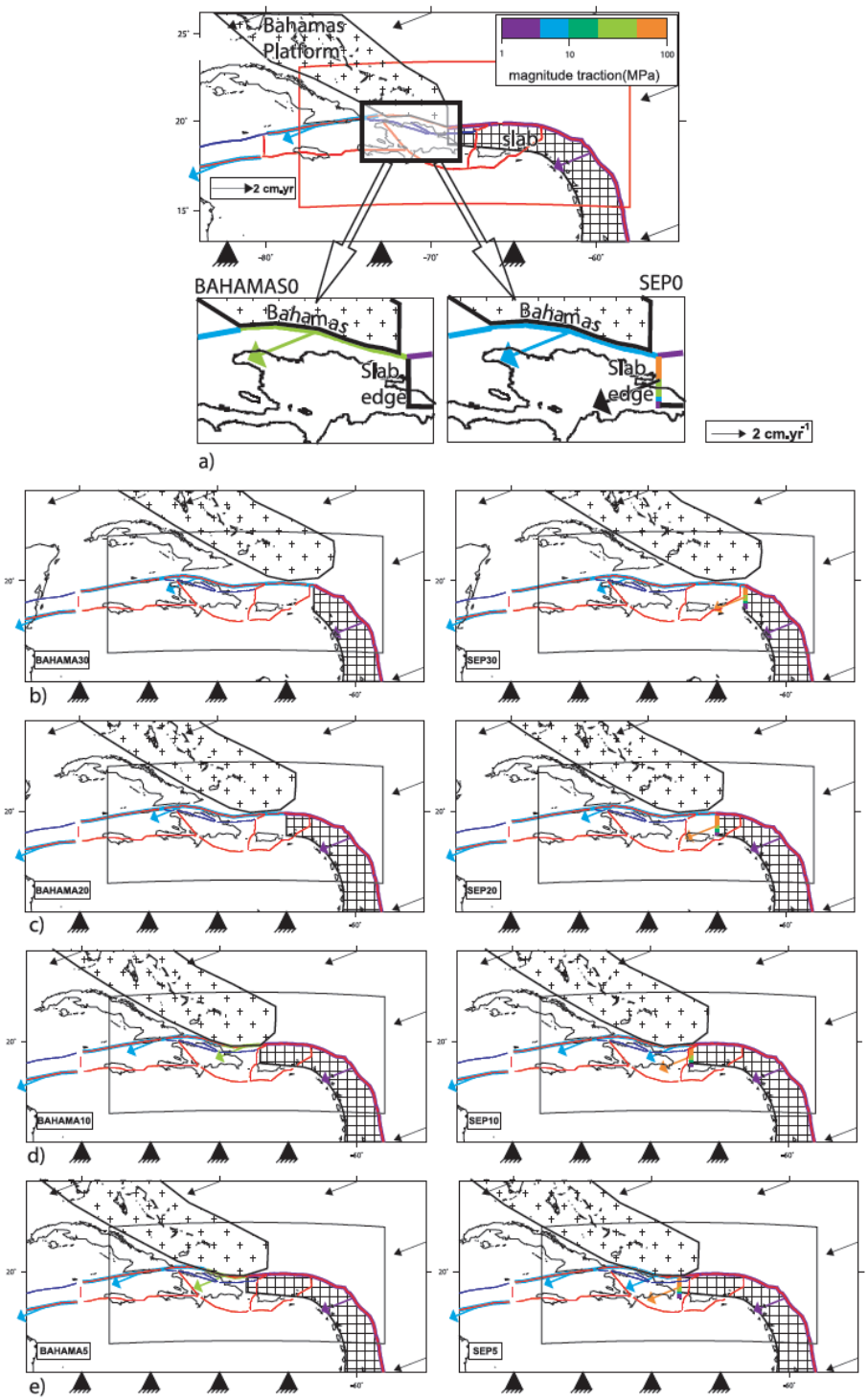

Figure 3

a) Boundary conditions for the models. Colored line segments denote magnitude of plate boundary friction (Pa) imposed. The arrows in the same color denote the direction of the imposed traction. Triangles at the bottom denote a zero displacement boundary condition; arrows at the top denote velocity boundary conditions. Thin colored lines denote fault type (red: 2 degrees of freedom, thrust fault. Blue: 1 degree of freedom, strike-slip fault). The subduction contact surface between the North America and Caribbean plates is striped and the red box shows the domain of the result figures. The insets show the different boundary conditions near the Bahamas and slab edge for the BAHAMA0 and SEP0 models.

b-e) Boundary conditions for the paleo-models at b) 30 Ma, c) 20 Ma, d) 10 Ma and e) 5 Ma. Symbols and colors are as in a). Positions of islands on the North America plate have been rotated back using the Euler pole from [*Leroy et al.*, 2000]. Results for the BAHAMAS models are presented in the left column, while Slab Edge Push models are in the right column.

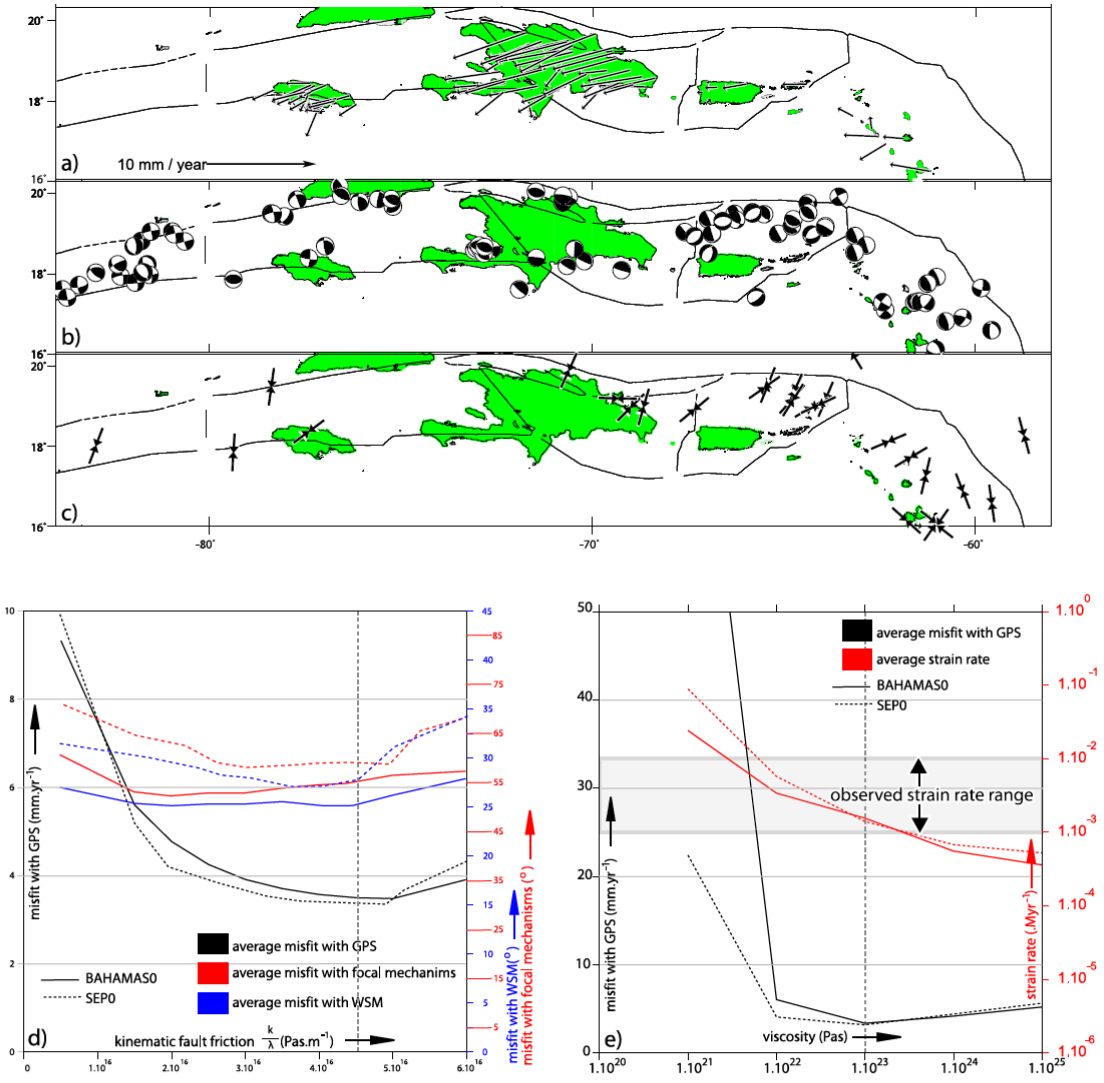

Figure 4

Comparison of observations and model results for the Present-day. **a)** GPS-derived velocities in the Caribbean reference frame. **b)** Crustal (0-33 km depth) focal mechanisms from the Centroid Moment Tensor (CMT) catalogue. **c)** Maximum compressive stress directions obtained from the World Stress Map [*Heidbach et al.*, 2008]. **d)** Misfit between model results and observations as function of kinematic fault friction. The calculation of the average misfit is explained in the text. We show the average misfit of modeled velocities with GPS-derived velocities (black line, black y-axis), average misfit of modeled principal stress direction with the World Stress Map (blue line, blue y-axis (right)) and average misfit of seismic slip (red line, red y-axis (right)). The solid lines represent the BAHAMA0 models, dotted line represent the SEP0 models. **e)** Misfit between model results and ob-

servations as a function of viscosity: Average misfit of modeled velocities with GPS-derived velocities (black line, black y-axis), average misfit of modeled principal stress direction with the world stress map (blue line, blue y-axis (right)) and average misfit of seismic slip (red line, red y-axis (right)). The solid lines represent the BAHAMA0 models, dotted line represent the SEP0 models.

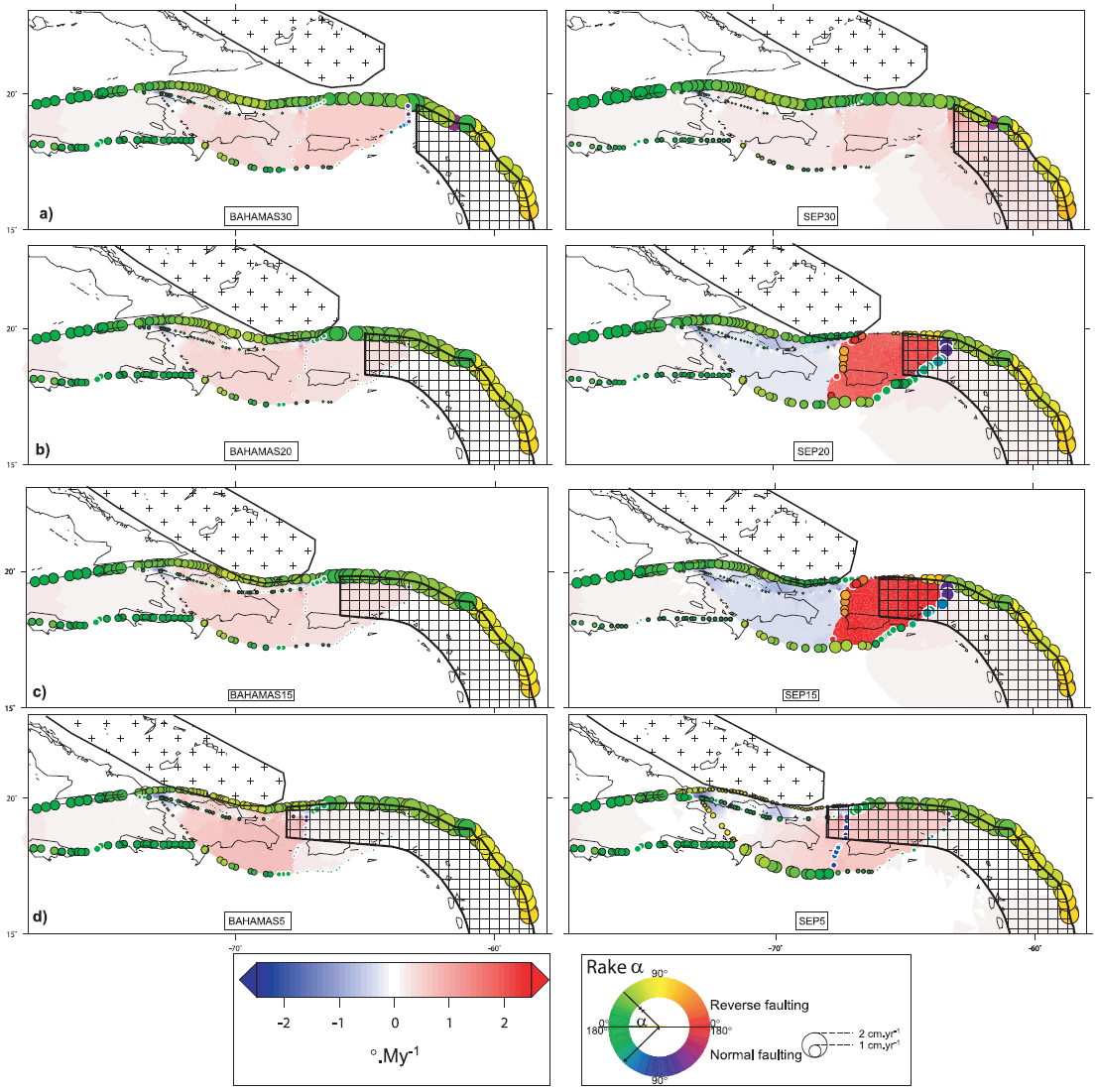

Figure 5

Rotation rate ($^{o}\cdot My^{-1}$) around a vertical axis and fault slip for the paleo-models in row **a)** 30 Ma, **b)** 20 Ma, **c)** 15 Ma and **d)** 5 Ma. Red colors denote CCW rotation rates and blue colors denote CW rotation rates. The color of the dots indicates the sense of relative motion on the faults. The size of the dots denotes fault displacement rate. Results for the Bahamas Collision models are presented in the left column, while the Slab Edge Push models are in the right column.

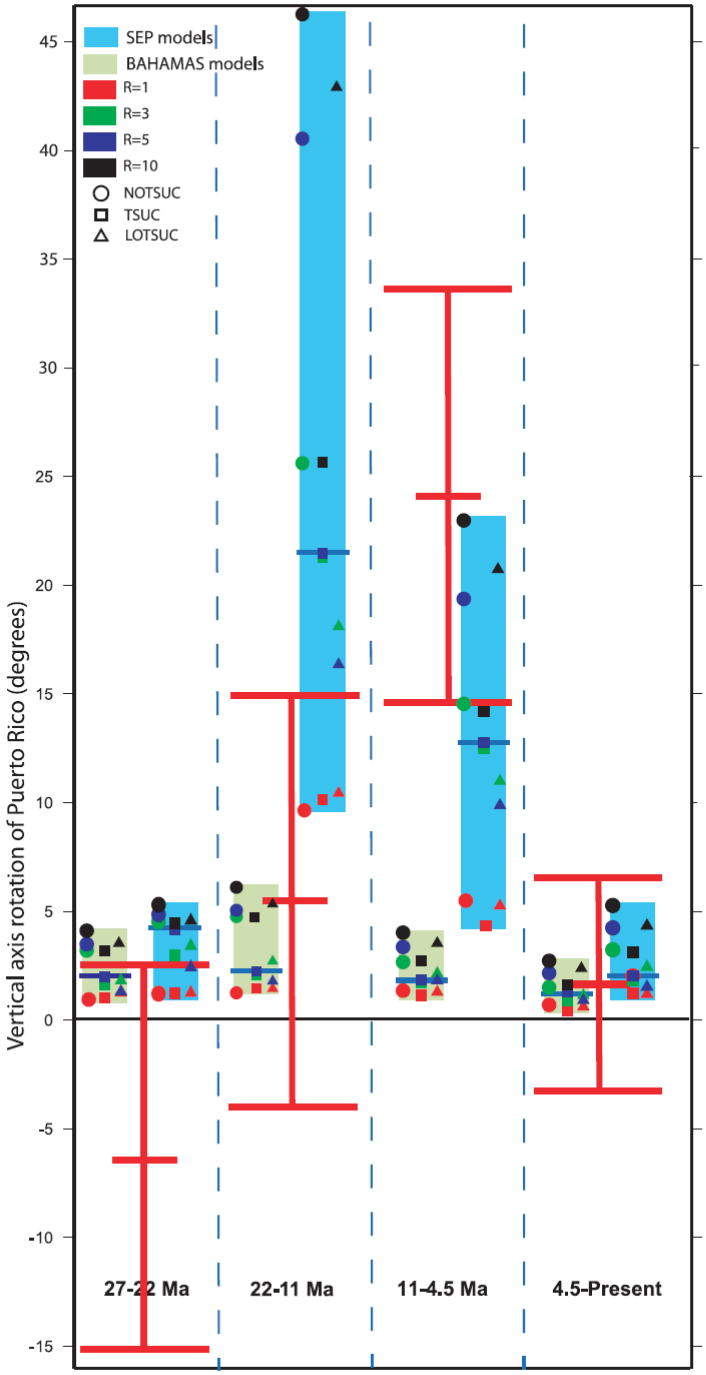

Figure 6

Observed amounts of rotation for Puerto Rico, during the time intervals of 27-22 Ma, 22-11 Ma, 11-4.5 Ma and 4.5 Ma-Present (Reid et al., 1991), compared with model results for the same time intervals. Thick red show observed rotations with error bars denoting the 90% confidence intervals associated with each observation (obtained from table 2 in Reid et al., 1991). Symbols in the blue boxes

represent rotations from Slab Edge Push models: different symbols refer to different line force sets (table 1). The grey-green box indicates the range of rotations obtained for the Bahamas Collision models, also for different line force sets. Blue horizontal lines denote the rotations for force set TSUC5. No single model reproduces the observed rotations (within uncertainty) at all intervals.

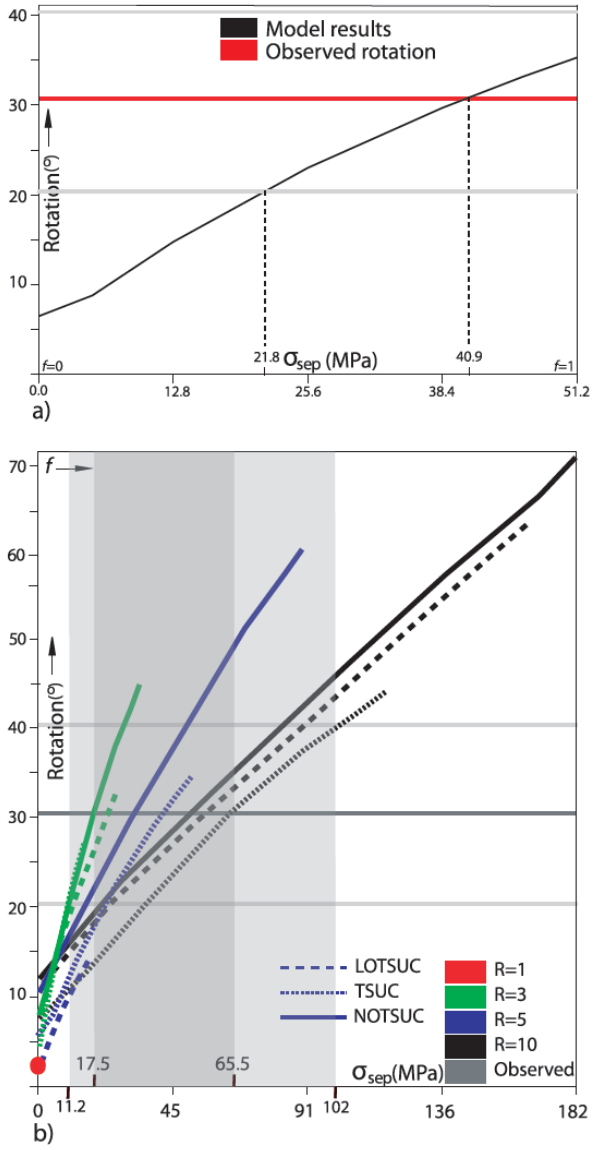

Figure 7

a) Total CCW rotation (22-0 Ma) for combinations of Slab Edge Push and Bahamas Collision for force set TSUC5 (black line). The relative contribution of the two mechanisms is parameterized by σ_{sep} (horizontal axis), the magnitude of the traction acting on the contact area between the slab edge and the Caribbean plate (Figure 3). Forcing is by Bahamas Collision only for $\sigma_{sep} = 0$. For larger values, Slab Edge Push also contributes to the forcing. The horizontal red line indicates the observed total rotation for 22-0 Ma (31°, solid line) and the grey lines denote the 90% confidence values. The total modeled rotation from 22 to 0 Ma matches the observations from the same period for

σ_{sep} =21.8 to 51.2 MPa.

b) Modeled total CCW rotation (22-0 Ma) as a function of σ_{sep}, for all line force sets in table 1. The gray horizontal line indicates the observed total rotation for 22-0 Ma (31°) and lighter grey lines denote its 90% confidence intervals Colors of the lines denote *R*, i.e. $\frac{F_{bah}}{F_{pbf}}$ (see text for details), the texture of the lines the amount of trench suction at the Southern Lesser Antilles. The dark gray area indicates the range for σ_{sep} that is needed to reproduce the observed 31° of CCW rotation (17.5 - 65.5 Mpa). The lighter gray area denotes the range for σ_{sep} that reproduces rotations that fall withing the 90% confidence range (11.2-102 MPa)

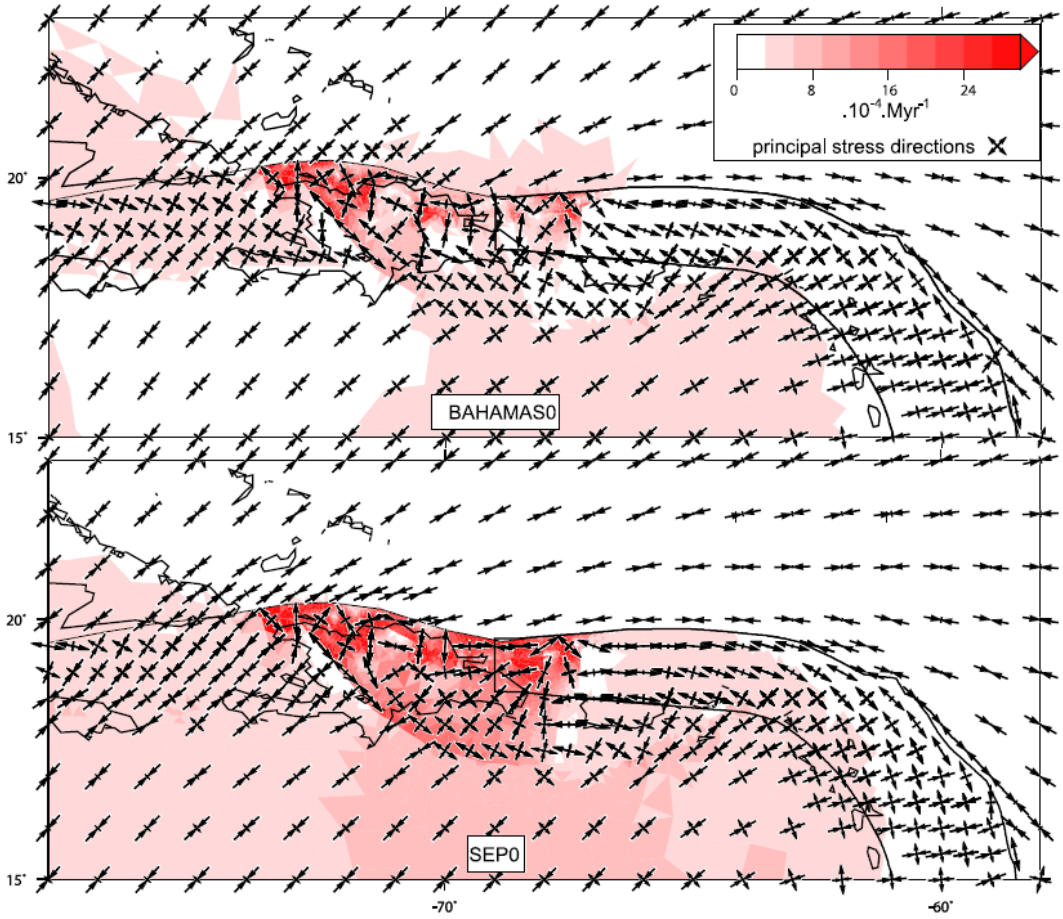

Figure A1

Results for models simulating Present-day tectonics. Colors in the figures are saturated. The left column shows the BAHAMA0 model results, the right column the SEP0 results.

a) Calculated effective strain rate (Myr^{-1}). The effective strain rate is defined as the second invariant of the strain rate tensor. Black crosses denote the principal strain rate directions.

b) Calculated uplift rate. The uplift rate is shown in $m \cdot Myr^{-1}$. Blue colors denote subsidence, red colors uplift. Black arrows denote the velocity field ($mm \cdot yr^{-1}$).

c) Rotation rate ($^{\circ} \cdot Myr^{-1}$) around a vertical axis. Red colors denote positive rotation rates (CCW) and blue colors denote CW rotation rates. The color of the dots indicates direction of fault slip relative to the fault. The size of the dots denotes the magnitude of fault displacement.

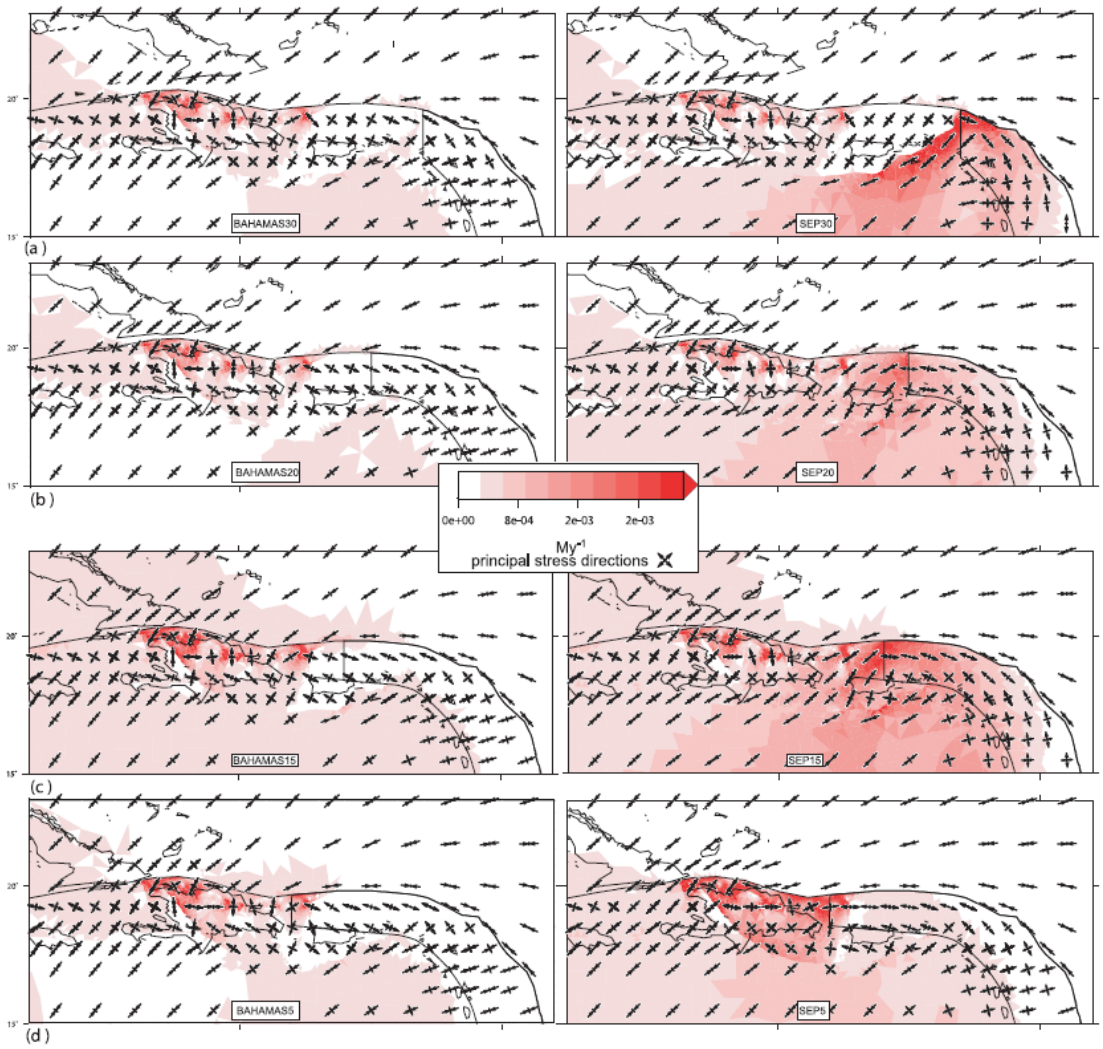

Figure A2

Effective strain rate (My^{-1}) and principal strain rate axes for the paleo-models. Black crosses denote the principal strain rate directions. The layout of the figure is identical to figure 5.

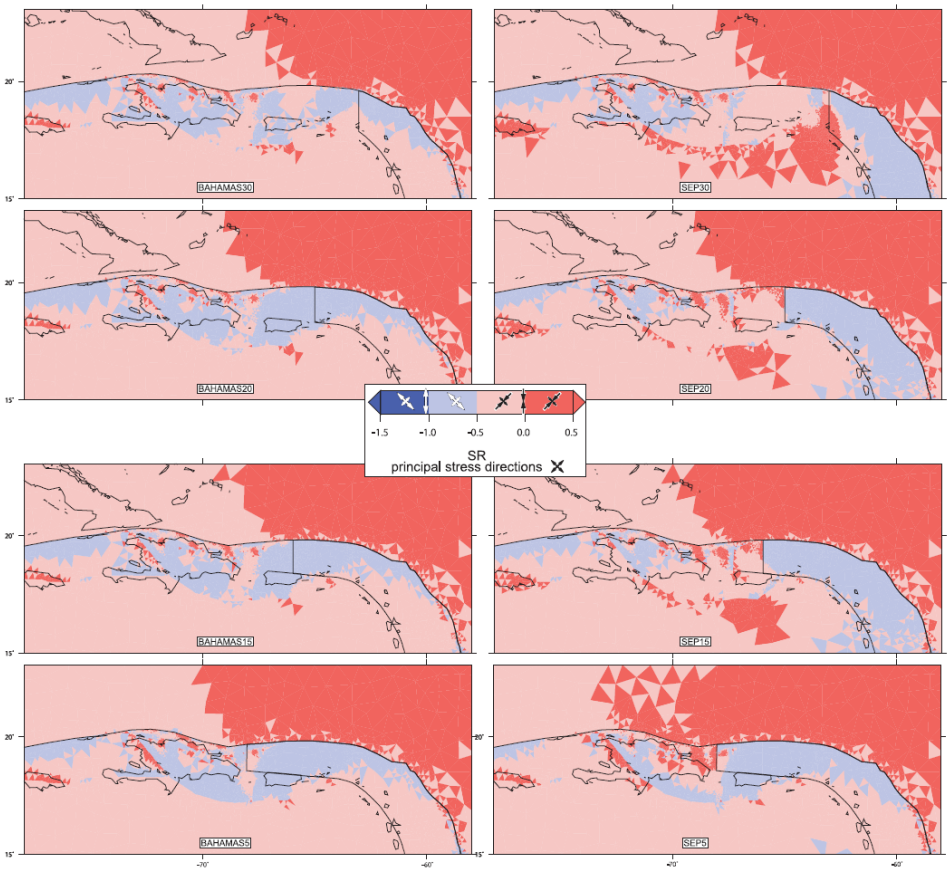

Figure A3

Stress ratio SR [*Álvarez-Gómez et al.*, 2008], defining the tectonic regime: uni- or bi-axial tension (SR < -1), transtension (-1 < SR < -0.5), pure strike-slip (SR=-0.5), transpression (-0.5 < SR < 0) and uni- or bi-axial compression (SR > 0). The layout of the figure is identical to Figure 5.

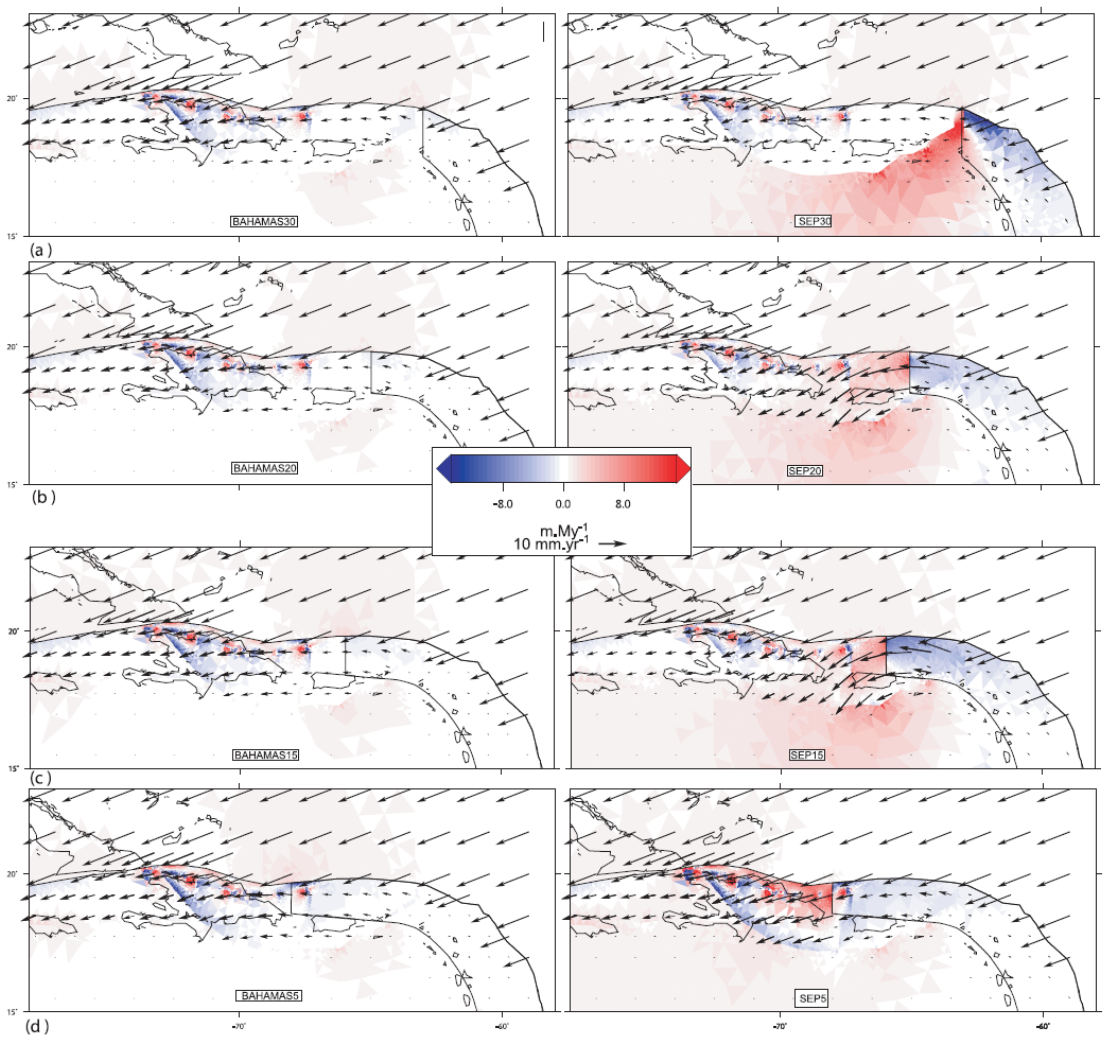

Figure A4

Modeled uplift rate and velocities for the paleo-models.

The uplift rate is shown in m·My^{-1}. Blue colors denote subsidence, red colors uplift. Black arrows denote the velocity field (mm·yr^{-1} The layout of the figure is identical to Figure 5.

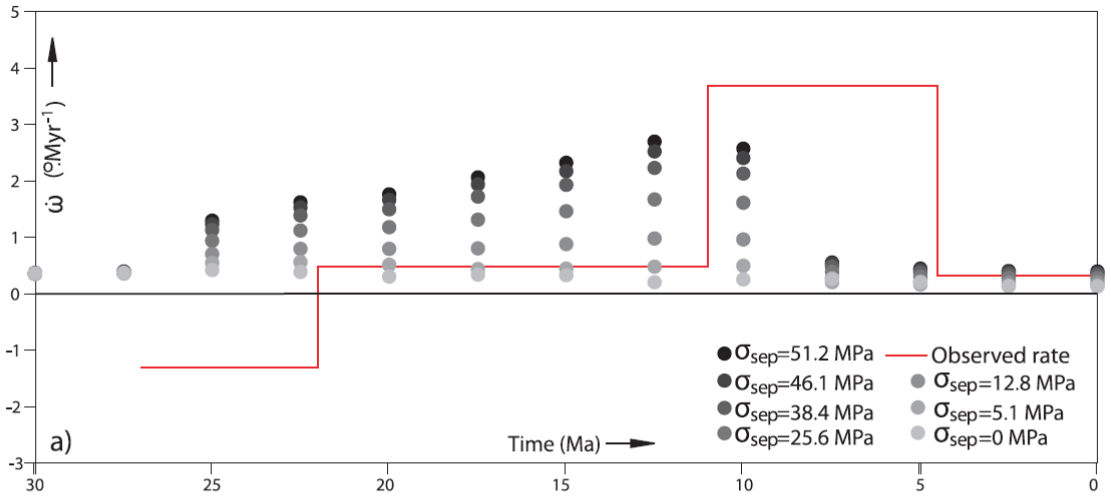

Figure A5

Modeled rotation rate compared with the observed rotation rate [*Reid et al.*, 1991] as a function of time (Myr). The color of the black to light-gray dots denotes the magnitude of the Slab Edge Push traction (σ_{sep}) used to construct the models. On the y-axis are the modeled rotation rates. The red line is the observed rotation rate.

Table 1

An overview of models representing the dynamics for the Caribbean plate [*van Benthem and Govers*, 2010]. The models differ in their assumptions of the relative magnitude of the Bahamas Collision force and the trench suction force at the Southern Lesser Antilles. Acronyms for the models are constructed as follows:

- NOTSUC: "NO Trench SUCtion"; No trench suction at the southern Lesser Antilles Trench.
- TSUC: "Trench SUCtion"; Trench suction at the southern Lesser Antilles Trench, modeled by an outward directed suction force of 45.10^{10} N/m.
- LOTSUC: "a LOT of trench SUCtion"; i.e. trench suction at the southern Lesser Antilles Trench, modeled by an outward directed suction force of 9.10^{11} N/m.
- The number stands for *R*, i.e. $\frac{F_{bah}}{F_{pbf}}$ (see text for details).

Model acronym	Trench suction at Southern Lesser Antilles	Relative magnitude of Bahamas force
NOTSUC1	0 Nm^{-1}	Equal to plate boundary friction
NOTSUC3	0 Nm^{-1}	3 x plate boundary friction
NOTSUC5	0 Nm^{-1}	5 x plate boundary friction
NOTSUC10	0 Nm^{-1}	10 x plate boundary friction
TSUC1	$6{\cdot}10^{11}$ Nm^{-1}	Equal to plate boundary friction
TSUC3	$6{\cdot}10^{11}$ Nm^{-1}	3 x plate boundary friction
TSUC5	$6{\cdot}10^{11}$ Nm^{-1}	5 x plate boundary friction
TSUC10	$6{\cdot}10^{11}$ Nm^{-1}	10 x plate boundary friction
LOTSUC1	$9{\cdot}10^{11}$ Nm^{-1}	Equal to plate boundary friction
LOTSUC3	$9{\cdot}10^{11}$ Nm^{-1}	3 x plate boundary friction
LOTSUC5	$9{\cdot}10^{11}$ Nm^{-1}	5 x plate boundary friction
LOTSUC10	$9{\cdot}10^{11}$ Nm^{-1}	10 x plate boundary friction

Table 2

Magnitudes of calculated line forces from Van Benthem and Govers (2010). The compositional buoyancy was kept at $4.0 \cdot 10^{12}$ N/m consistent with the crustal structure in the Caribbean. Values for the basal drag were kept as close to zero as possible [*van Benthem and Govers*, 2010]

Model:	F_{pcr} (10^{11} Nm^{-1})	F_{tf} (10^{11} Nm^{-1})	F_{bah} (10^{11} Nm^{-1})	Basal drag (10^5 Pa)
NOTSUC1	4.20	6.11	0.0	-4
NOTSUC3	4.36	2.86	8.72	-3
NOTSUC5	3.34	2.32	13.76	-2
NOTSUC10	2.02	3.82	18.18	-1
TSUC1	5.54	5.43	0.0	-1.5
TSUC3	2.50	3.39	5.01	-0.5
TSUC5	2.02	2.64	8.08	0
TSUC10	1.30	3.11	11.7	1.0
LOTSUC1	4.28	4.44	0	-0.5
LOTSUC3	3.32	3.82	6.64	0.5
LOTSUC5	0.82	0.63	3.28	1.0
LOTSUC10	1.84	2.76	16.56	2.0

Table 3

An overview of symbols for forces and derived quantities (tractions and torques) used.

Symbol	Magnitude	Direction	Description
$\mathbf{F_{bah}}$	F_{bah}	$\hat{F}_{bah}$	Bahamas Collision force
$\mathbf{F_{sep}}$	F_{sep}	$\hat{F}_{sep}$	Slab Edge Push force
$\boldsymbol{\sigma}_{\mathbf{bah}}$	σ_{bah}	$\hat{\sigma}_{bah}$	Bahamas Collision traction
$\boldsymbol{\sigma}_{\mathbf{sep}}$	σ_{sep}	$\hat{\sigma}_{sep}$	Slab Edge Push traction
$\mathbf{T_C}$	T_C	$\hat{T}_C$	Combined torque of Slab Edge Push and Bahamas Collision

Table 4

Misfit of Present day models with observational constraints. $\Delta\alpha$ (^{o}) is the average misfit with the World Stress Map, $\Delta\theta$ (^{o}) is the average misfit with fault slip, derived from focal mechanisms from the Centroid Moment Tensor project and Δv ($mm.yr^{-1}$) is the average misfit with GPS-derived velocities.

	$\Delta\alpha$ (^{o})	$\Delta\theta$ (^{o})	Δv ($mm \cdot yr^{-1}$)
Bahamas	25.7	55.7	3.41
Slab Edge Push:	28.1	58	3.40

Table 5

The total slip (meters) on faults for the Slab Edge Push and Bahamas Collision models.

Fault name	Total slip (m) Bahama models	Total slip (m) Slab Edge Push models	Total observed slip (m)
Muertos Trough	88,162	152,053	40,000-150,000
Mona Rift	54,946	115,170	6,100
Anegada FZ	51,588	101,550	40,000-150,000
Enriquillo-Plantain-Garden FZ	116,295	91,233	30,000-50,000
Fault name	Average slip rate Bahama models	Average slip rate Slab Edge Push models	Average observed slip rate
Septentrional FZ	4.2 mm·yr^{-1}	4·3 mm.yr^{-1}	9±3 mm·yr^{-1}